

# Evidence of subsurface control on the coevolution of hillslope morphology and runoff generation

David G Litwin<sup>1</sup> and Ciaran J Harman<sup>2</sup>

<sup>1</sup>Helmholtz-Zentrum Potsdam - Deutsches Geoforschungszentrum

<sup>2</sup>Johns Hopkins University

September 15, 2024

1 **Evidence of subsurface control on the coevolution of**  
2 **hillslope morphology and runoff generation**

3 **David G. Litwin<sup>1,2</sup>, Ciaran J. Harman<sup>2,3</sup>**

4 <sup>1</sup>Earth Surface Process Modelling, Helmholtz Center GFZ Potsdam, Potsdam, DE

5 <sup>2</sup>Department of Environmental Health and Engineering, Johns Hopkins University, Baltimore, MD, USA

6 <sup>3</sup>Department of Earth and Planetary Science, Johns Hopkins University, Baltimore, MD, USA

7 **Key Points:**

- 8 • We test theoretical predictions about the relationship between hillslope length and  
9 relief, saturated area, and transmissivity  
10 • Comparing two watersheds, we find lower transmissivity is associated with shorter  
11 hillslopes and larger variably saturated areas  
12 • Hydrogeomorphic modelling suggests that subsurface properties drive the coevo-  
13 lution of differences between the sites

---

Corresponding author: David G. Litwin, [david.litwin@gfz-potsdam.de](mailto:david.litwin@gfz-potsdam.de)

## Abstract

Topography is a key control on runoff generation, as topographic slope affects hydraulic gradients and curvature affects water flow paths. Simultaneously, runoff generation shapes topography through erosion, affecting landscape morphology over long timescales. Previous modeling efforts suggest that subsurface hydrological properties, relative to climate, are key mediators of this relationship. Specifically, when subsurface transmissivity and water storage capacity are low, (1) saturated areas and storm runoff should be larger and more variable, and (2) hillslopes shorter and with less relief, assuming other geomorphic factors are held constant. However, it remains uncertain whether subsurface properties can exert such strong controls on emergent properties in real landscapes. We compared emergent hydrological function and topography in two watersheds with very similar climatic and geologic history, but very different subsurface properties due to contrasting bedrock lithology. We found that hillslopes were systematically shorter and saturated areas more dynamic at the lower transmissivity site. To test whether these features could be the result of coevolution between topography, hydrological function, and subsurface properties, we estimated all parameters of a coupled groundwater-landscape evolution model for each site. Limitations were revealed in the model's ability to reproduce aspects of morphology and hydrologic behavior, however, model results suggested differences in drainage density and variably saturated area between the sites could be explained by differences in subsurface properties, and not by differences in geomorphic process rates alone. This work demonstrates one way subsurface hydrology can profoundly affect landscape evolution.

## Plain Language Summary

In many humid landscapes, runoff is generated by water that flows through the shallow subsurface from ridges to valleys, eventually emerging and draining to rivers. When subsurface capacity to move water is greater, more water can be transported downslope before surface runoff begins. Surface water may cause erosion, which shapes topography over millions of years. We previously developed a computer model based on these principles and showed that subsurface capacity to store and transmit water affects both runoff generation and topographic evolution. Lower capacity results in more extensive surface runoff and shorter hillslopes, when all other factors are held constant. Here we tested this by comparing two watersheds that differ primarily in their bedrock composition, which affects subsurface water storage and transmissivity. We found that the low transmissivity site experienced more widespread surface runoff in response to precipitation, and had shorter hillslopes, supporting our predictions. We set up computer models for both sites, which suggested that subsurface differences are necessary to explain observed differences in runoff and topography. Finally, we discuss some key limitations of the model that could be improved upon in future attempts to understand how hydrology affects the long-term evolution of Earth's surface.

## 1 Introduction

### 1.1 Background

It has long been understood that there is a close, two-way connection between runoff and the topographic form of landscapes. Topography influences surface and subsurface water flow paths and supplies the elevation component of hydraulic head, while erosion by water shapes landscapes over long timescales. Horton (1945) suggested that there is something valuable to learn about how places work hydrologically by considering this coupling. In particular, such coevolution may be useful for understanding and predicting catchment hydrological function (Troch et al., 2015).

62 Unfortunately, the vastly different timescales of runoff and evolution of channel net-  
63 works via erosion has made it challenging to study the coevolution of hydrological and  
64 geomorphic states and fluxes. Hydrologists studying runoff generation usually assume  
65 that landscape form is fixed, while geomorphologists studying landscape evolution usu-  
66 ally assume hydrology can be reduced to a few parameters that capture how hydrocli-  
67 mate affects the efficiency of bedrock erosion and sediment transport.

68 However, recent advances in modeling and the availability of high performance com-  
69 puters have made it possible to couple hydrologic and geomorphic models, and exam-  
70 ine the evolution of hydrologic and geomorphic states together. Litwin et al. (2022) used  
71 a shallow aquifer model to generate saturation excess runoff from steady recharge, and  
72 used the runoff to drive fluvial incision in a streampower-plus-diffusion landscape evo-  
73 lution model, called DupuitLEM. Litwin et al. (2024) extended DupuitLEM to exam-  
74 ine the emergence of variable source area hydrology by adding stochastic precipitation  
75 and a simple representation of the vadose zone, thus capturing more realistic hydrologic  
76 dynamics.

77 According to that model subsurface thickness and permeability are important con-  
78 trols on runoff, and consequently, the degree of drainage dissection and length of hill-  
79 slopes (Figure 1). Subsurface structure in DupuitLEM is represented by a single layer  
80 of constant thickness, but a cascading vadose zone model allows it to resolve vertical vari-  
81 ations in water content resulting from root water uptake, and the non-linear threshold-  
82 like spatial variations in the relationship between rainfall infiltration and groundwater  
83 recharge. The water table position responds to recharge from the vadose zone, and lat-  
84 eral flow calculated using Dupuit-like assumptions. A large subsurface thickness and per-  
85 meability therefore endows a model landscape with not only the ability to rapidly drain  
86 saturated storage, but also the ability to absorb storm event rainfall in the vadose zone,  
87 especially when the evapotranspiration rate was also high relative to rainfall. The model  
88 showed that these characteristics resulted in less saturation excess overland flow com-  
89 pared to landscapes with poor subsurface drainage, as saturated areas were smaller and  
90 less responsive to storm events. Less surface runoff means less water-driven erosion, which  
91 means that at geomorphic steady state (when uplift balances erosion) diffusive hillslope  
92 erosion processes must be larger to compensate. The result is a landscape with higher  
93 relief and less drainage dissection (e.g., Perron et al., 2008).

94 While these model results indicate that the subsurface is a key link between topog-  
95 raphy and runoff generation, it is unclear whether these relationships can be observed  
96 in real landscapes. While field studies have shown that subsurface properties and topog-  
97 raphy have effects on hydrologic function (e.g., Prancevic & Kirchner, 2019; Jencso &  
98 McGlynn, 2011), relationships between subsurface properties and topography remain elu-  
99 sive (Luo et al., 2016; Sangireddy et al., 2016). Furthermore, it has proven challenging  
100 to show that such a relationship is the result of coevolution with hydrology (Yoshida &  
101 Troch, 2016). This lack of clear relationships is to be expected because hydrology, con-  
102 ditioned by climate, is only one connection between the subsurface and topography. Other  
103 controls include lithology and tectonic setting, which affect the styles and efficiencies of  
104 weathering, sediment particle size, and sediment transport; and vegetation, which alters  
105 subsurface properties and sediment transport efficiency through root growth, and hydro-  
106 logic partitioning through evapotranspiration (Brantley et al., 2017; Collins & Bras, 2010).

107 In this paper we will look for evidence to support the hypothesis that subsurface  
108 thickness and permeability are important controls on surface topography (particularly  
109 relief and drainage density). We will apply the model of Litwin et al. (2024) to two lo-  
110 cations where confounding differences are minimized, and there is a contrast in both the  
111 degree of topographic dissection and the subsurface properties. We aim to avoid calibra-  
112 tion, relying instead in field observations, literature values, and topographic analysis to  
113 parameterize the model.

114 If the model is able to reproduce the distinct hydrologic and geomorphic proper-  
 115 ties of each site, this will lend strong credence to the arguments drawn from the model  
 116 about how they are coupled, and the importance of subsurface properties in modulat-  
 117 ing that coupling. However, parameter uncertainty makes it very possible that the model  
 118 will not reproduce the observed geomorphic length scales and hydrologic behaviour pre-  
 119 cisely. It is also possible that the process mechanisms we have chosen to encode in the  
 120 model are not actually the processes most important at these sites (we will discuss this  
 121 possibility later). If the model does not match the observations, or does so for the wrong  
 122 reasons, it still allows us to examine how sensitive model predictions are to subsur-  
 123 face properties given the realistic reference parameters the two sites provide. If the dif-  
 124 ference in model predictions between the sites align in magnitude and direction with ob-  
 125 servations from these sites this will provide (weaker, but defensible) support for the the-  
 126 sis.

## 127 1.2 Approach

128 We selected two sites where contrasting lithology results in a strong contrast in sub-  
 129 surface properties, but climatic and tectonic histories are similar because of their prox-  
 130 imity. Our first site, Druids Run, is underlain by serpentine bedrock that forms thin rocky  
 131 soil, while the second site, Baisman Run, is underlain by schist that weathers to form  
 132 deep, permeable soil and saprolite. We will assume that the present hydrological func-  
 133 tion is adjusted to the watershed geomorphology, and that the terrain approximates a  
 134 geomorphic steady-state, as suggested by (Pavich, 1989).

135 Given these differences in subsurface properties, insights gained from the analysis  
 136 in Litwin et al. (2024) lead us to hypothesize that:

- 137 1. Saturated areas and storm runoff are larger and more variable in time at Druids  
 138 Run than Baisman Run, and
- 139 2. Hillslopes are shorter and have less relief at Druids Run than Baisman Run.

140 Here we examine these hypotheses in three steps. First, we characterize the hydrolog-  
 141 ical function and morphology of the two sites and evaluate whether they support these  
 142 hypotheses. Second, we ask whether these differences could be accounted for by coevo-  
 143 lution between runoff generation and erosion as conceptualised in our model. To do this  
 144 we fully parameterize the landscape evolution model used in Litwin et al. (2024) with-  
 145 out calibration and compare its predictions to the site properties. Third, we test whether  
 146 subsurface hydrological differences are indeed the most important factors (or whether  
 147 differences in other geomorphic properties can account for the different site morphol-  
 148 ogies) by performing a simple sensitivity analysis in which we swap the geomorphic pro-  
 149 cess variables between the two sites while retaining the hydrologic and subsurface prop-  
 150 erties. The results reveal the relative importance of variations in subsurface hydrology  
 151 relative to geomorphic process rates in explaining differences in emergent morphology  
 152 and hydrologic function at these sites.

## 153 2 Materials and Methods

### 154 2.1 Site descriptions

155 Our study sites are located in the Piedmont physiographic province, north of Bal-  
 156 timore, Maryland. The climate is humid, with a mean annual precipitation of approx-  
 157 imately 1150 mm and mean annual potential evapotranspiration of approximately 750  
 158 mm. There is no pronounced seasonality in precipitation, less than 5% of which falls as  
 159 snow. Baisman Run is a 381 ha watershed in Oregon Ridge Park, defined by an outlet  
 160 at (39.4795 N, 76.6779 W). Druids Run is a 107 ha watershed located in Soldiers Delight  
 161 Natural Environment Area, and is defined by an outlet at (39.4171 N, 76.8523 W). The

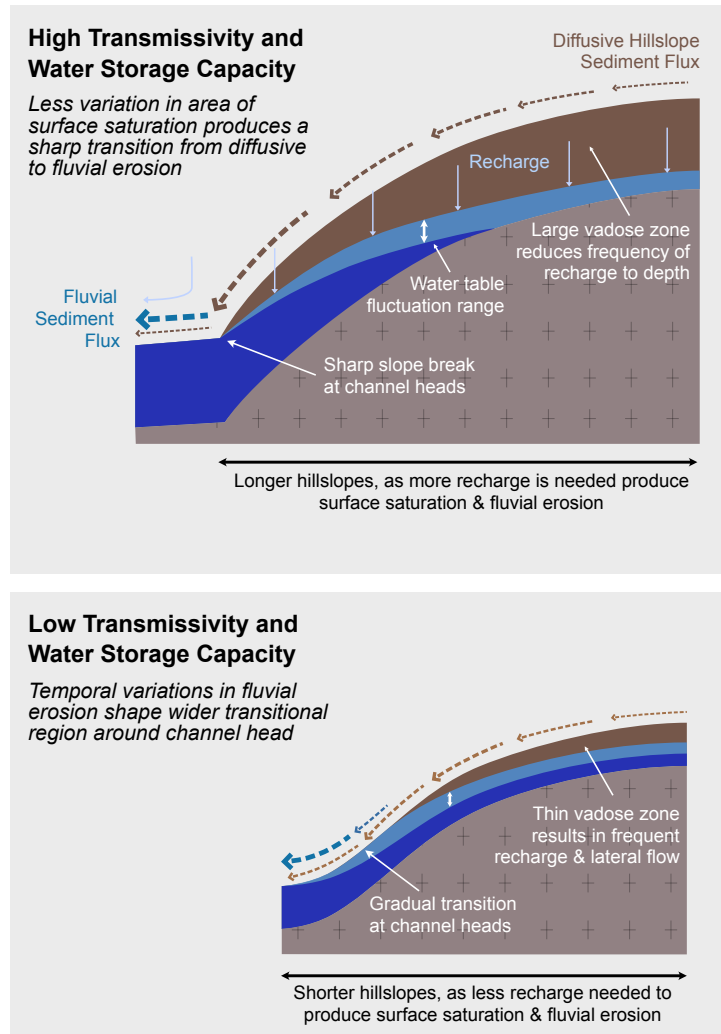


**Figure 1.** Conceptual figures showing a contrast in morphology and water table from ridge to channel head predicted by DupuitLEM. Gravity driven hillslope sediment flux moves material downslope proportional to the topographic gradient (brown dashed arrows). Water-driven fluvial erosion occurs where there is surface water, generated by precipitation on saturated areas and exfiltration (blue dashed arrows). When transmissivity and water storage capacity (drainable porosity integrated with depth) relative to storm event size are large, the subsurface can support long water flow paths before exfiltration, and the position where the water table intersects the surface is relatively static with time. When transmissivity and storage capacity are lower, hillslopes are shorter and the water table is more sensitive to time-varying recharge, such that the zone of surface water discharge and erosion varies in the vicinity of the channel head.

162 watersheds are 16 km apart, and are at approximately the same elevation (52 m and 56  
 163 m above sea level respectively). Both watersheds drain to the Chesapeake Bay; Baisman  
 164 Run drains via the Gunpowder River and Druids Run via the Patapsco River. Baisman  
 165 Run has been monitored extensively as part of the Baltimore Ecosystem Study, and more  
 166 recently as part of several projects aimed at improving understanding of deeply weath-  
 167 ered critical zones (Putnam, 2018; Cosans, 2022). Druids Run has no prior description

168 or study. It is unnamed in the National Hydrography Dataset, so we unofficially named  
 169 it in honor of a local group of druids that meet in the watershed.

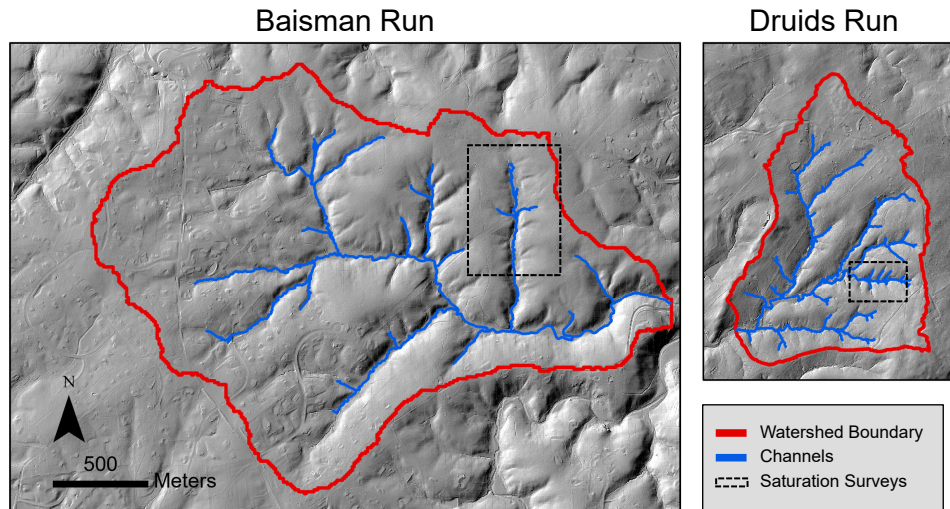


**Figure 2.** Hillshades of Baisman Run and Druids Run with the watershed boundary and channel network delineated with the DrEICH algorithm. Areas where we conducted saturation surveys (see Figure 5) are shown in dashed black boxes. The two sites are to scale, revealing the difference in their size and drainage dissection.

170 Baisman Run is underlain by the Loch Raven Schist (Crowley et al., 1975), a Cambrian-  
 171 Devonian mica schist that has weathered to form deep, moderately permeable soil and  
 172 saprolite. Drilling and geophysical measurements show that at the ridge, the depth to  
 173 the saprolite-bedrock transition is  $\approx 15$  m and weathered bedrock extends several tens  
 174 of meters further (Cosans, 2022). The depth to the saprolite-bedrock transition is much  
 175 shallower in valley bottoms,  $\approx 0-2$  m, as there are some bedrock outcrops appearing  
 176 in channels (Cosans, 2022). The USDA maps the primary soils in the watershed as well-  
 177 drained, loam to silt-loam textured with depth to water table and confining layer greater  
 178 than 200 cm. Valley bottoms soils are poorly drained, with hydric-classified soils com-  
 179 posing  $\approx 3\%$  of the watershed (Staff & Natural Resources Conservation Service, United  
 180 States Department of Agriculture., 2023). Agriculture was historically present in the east-  
 181 ern headwaters, where there is now suburban development, and a homestead and tree  
 182 farm were historically present in the Pond Branch sub-watershed (Cleaves et al., 1970).  
 183 The remainder of the watershed has been relatively undisturbed since the 1950s and to-  
 184 day supports a mature deciduous forest.

185 Druids Run is primarily underlain by the Soldiers Delight Ultramafite (Guice et  
 186 al., 2021). Soils are primarily classified as chrome silt loam, and are generally thin with  
 187 a strong permeability contrast at the base of the A horizon (at an average depth of 46  
 188 cm). Ridgetop soil is rocky and can be as thin as 5 cm, and exposed bedrock is common  
 189 near channel heads. In valley bottoms, alluvium and organic material accumulate to thick-  
 190 nesses around 1 m. Hydric-classified soils are found in some valley bottoms and compose  
 191  $\approx 1\%$  of the watershed (Staff & Natural Resources Conservation Service, United States  
 192 Department of Agriculture., 2023). The Soldiers Delight Ultramafite is host to a “ser-  
 193 pentine barrens” ecosystem, which consists primarily of grasses and shrubs with some  
 194 areas supporting hardwood and conifer trees. The Soldiers Delight area was mined for  
 195 chromite in the 19th and 20th century. Several small pits are present near ridge crests

196 in Druids Run, and placer mining may have occurred in the valley bottoms, but the ef-  
197 fects of this appear to be minimal in this watershed. Some structures and two small ponds  
198 are present in the upper portion of Druids Run, but most of the watershed is free from  
199 development.

## 200 2.2 Hydrological data

201 We combined existing hydrological data with new measurements of precipitation,  
202 streamflow, and saturated areas. Instantaneous precipitation rates were measured from  
203 June 2022 to February 2023 at a weather station located in an open field approximately  
204 0.8 km north of Baisman Run. An identical unit was installed in an open area in Druids  
205 Run, which recorded instantaneous precipitation from April 2022 to February 2023. The  
206 stream gage at Baisman Run is operated and maintained by the U.S. Geological Survey  
207 (Gage 01583580). We established a new stream gage at Druids Run for this project.

208 The Druids Run stream gage is located at an existing concrete culvert crossing the  
209 stream channel. In April 2022 we installed a PVC housing on the concrete structure ap-  
210 proximately 2 m from the culvert inlet. We measured water stage with a Solinst Lev-  
211 elogger pressure transducer within that housing, and corrected for atmospheric pressure  
212 with a Solinst Barologger. The pressure transducer operated until the device failed in  
213 October 2022. Periodic discharge measurements were made to construct a rating curve.  
214 Low flows were measured with salt dilution gaging recorded with a HOBO conductiv-  
215 ity logger, and high flows were measured using an OTT MF Pro electromagnetic cur-  
216 rent profiler. A power law model fit the stage-discharge data well, as shown in Figure  
217 S1.

218 While we do not have site-specific discharge uncertainty estimates, prior studies  
219 suggest reasonable and similar values. The U.S. Geological Survey reports gage discharge  
220 error is typically 3-6%, and rarely up to 20% (Sauer & Meyer, 1992). Schmadel et al.  
221 (2010) conducted an in-depth uncertainty analysis of discharge estimated from a dilu-  
222 tion gaging procedure very similar to ours and found approximately 8% error.

223 We surveyed limited areas of both watersheds manually for saturation conditions  
224 between April 2022 and March 2023. At Baisman Run, the surveys were conducted in  
225 the headwaters of the Pond Branch sub-watershed. At Druids Run, they were conducted  
226 in a headwater catchment near the eastern watershed boundary. We measured satura-  
227 tion at points along predefined transects, and returned to the approximate (but not ex-  
228 act) positions for each survey. We selected transects to balance capturing a range of hill-  
229 slopes, zero- and first-order channels, while covering a small enough area to avoiding sig-  
230 nificant changes in saturation over the course of a measurement campaign. Saturation  
231 was measured by walking the transects, and pushing a rebar rod approximately 2 cm into  
232 the ground and moving the rod up and down in the shallow hole. Points along these tran-  
233 sects were recorded as not saturated if no squishing sound was heard (N), soil-saturated  
234 if a squishing sound was heard (Ys), ponded (Yp), or flowing (Yf) if water was observed  
235 on the surface. Three close locations were measured at each point on the transect, and  
236 the highest category in this hierarchy was recorded as the value (e.g., if two points did  
237 not squish, but one did, the recorded class would still be Ys). This procedure was repeated  
238 under different discharge and moisture conditions.

## 239 2.3 Hydrological analysis

240 Valuable information about contributing areas can be extracted from rainfall and  
241 runoff timeseries. The event runoff ratio, defined as the ratio of the total event runoff  
242 to event precipitation, can approximate the proportion of the watershed contributing storm  
243 runoff (e.g., O'Loughlin, 1986). To calculate event runoff, we first separated the discharge  
244 timeseries into baseflow and quickflow using the graphical approach described by Hewlett



245 and Hibbert (1967). Because hydrograph separation only delineates by timescale of re-  
 246 sponse (fast versus slow), the resulting event runoff does not necessarily derive from a  
 247 particular runoff pathway, such as runoff from saturated areas. Still, the event runoff ra-  
 248 tio can provide an indication of the relative watershed connectivity that drives rapid runoff  
 249 response to rainfall.

250 Using the method of Hewlett and Hibbert (1967), baseflow is equal to discharge  
 251 and quickflow is zero until discharge increases at a rate faster than  $0.000546 \text{ m}^3 \text{ s}^{-1} \text{ km}^{-2}$   
 252  $\text{h}^{-1}$ . Baseflow continues to increase at this rate until discharge declines and is equal to  
 253 baseflow. Storm events are periods where quickflow is greater than zero and the rise is  
 254 associated with precipitation. Corresponding precipitation events start  $t_0$  hours before  
 255 event quickflow begins, and end  $t_1$  hours before discharge returns to baseflow, where  $t_0$   
 256 and  $t_1$  are fixed values for each site. By examining precipitation and discharge timeseries,  
 257 we found that  $t_0 = 2$  hours and  $t_1 = 1$  hour were appropriate for Druids Run, and  
 258  $t_0 = 6$  hours and  $t_1 = 2$  hours were appropriate for Baisman Run. We excluded runoff  
 259 events shorter than 6 hours because these generally had small discharge responses rela-  
 260 tive to noise in the timeseries.

While the runoff ratio provides a signature of contributing area, the saturation dataset  
 provides a direct means to assess the variability of saturated areas. The saturation sur-  
 veys yielded categorical data that vary with topographic position and catchment discharge.  
 To develop quantitative insights from the dataset, we first created a binary classification  
 of whether points were not saturated (N) or saturated (Ys, Yp, Yf). We then used lo-  
 gistic regression to generalize our discrete measurements to predictions of how satura-  
 tion probability  $p$  varies in space, assuming similarity with topographic (wetness) index  
 $TI = \frac{A}{v_0|\nabla z|}$  (Beven & Kirkby, 1979), and in time assuming similarity with baseflow  
 discharge  $Q_b$ :

$$\log\left(\frac{p}{1-p}\right) = \alpha_0 + \alpha_1 \log\left(\frac{A}{v_0|\nabla z|}\right) + \alpha_2 \log\left(\frac{Q_b}{A_{tot}}\right) \quad (1)$$

261 where  $A(x, y)$  is the area upslope of a contour width  $v_0$ ,  $|\nabla z(x, y)|$  is the topographic slope,  
 262 and  $A_{tot}$  is the total watershed area. The model parameters are  $\alpha_0$ ,  $\alpha_1$ , and  $\alpha_2$ .

263 To calculate topographic index, we first resampled the DEM to 5 m resolution to  
 264 smooth over roughness in the high resolution DEM and to reflect the uncertainty in the  
 265 positioning data of our saturation surveys. The resampling approach is also consistent  
 266 with our measurement scheme, in which we labeled locations based upon the highest satu-  
 267 ration class observed in a small vicinity. We calculated upslope area using the  $D_\infty$  al-  
 268 gorithm, and slope using the same 10 m footprint used to calculate hilltop curvature. While  
 269 our regression model calls for the use of baseflow discharge, we used the total discharge,  
 270 as all of our samples were taken during baseflow or recession periods. This was also nec-  
 271 essary because the timeseries of discharge at Druids Run did not overlap all the satu-  
 272 ration surveys. For consistency, we used instantaneous discharge measurements from im-  
 273 mediately before the surveys began. At Druids Run, we made these measurements using  
 274 dilution gaging; at Baisman Run, we used instantaneous discharge from the USGS  
 275 gage.

## 276 2.4 Hillslope length and relief

277 We conducted geomorphic analyses using a lidar-derived digital elevation model  
 278 with 0.76 m resolution, which was collected in 2015 and is publicly available from Bal-  
 279 timore County. We conducted all topographic analyses using LSDTopoTools (S. Mudd  
 280 et al., 2022). To determine hillslope length and relief, we began by identifying the chan-  
 281 nel networks at both sites using the DrEICH algorithm (Clubb et al., 2014). DrEICH  
 282 uses  $\chi$ -analysis (Perron & Royden, 2013) to locate channel heads at the transition point  
 283 from linear channel segments to nonlinear hillslope segments in  $\chi$ -elevation space.  $\chi$ -analysis  
 284 is discussed in more detail in Section 2.7.2. We adjusted the DrEICH model parameters

285 such that the predicted channel network matched observed channel network in the sub-  
286 watersheds where we measured saturation. The channel network in these areas was ob-  
287 served visually in the field as the extent of fluvial incision with clear connection to larger  
288 channel baselevel. We then used the channel network to identify hilltops, which are de-  
289 fined as edges shared by watersheds with the same Strahler stream order (Hurst et al.,  
290 2012). Finally, we calculated hillslope length as the steepest descent distance from each  
291 hilltop point to the nearest channel point, and hillslope relief as the hilltop elevation above  
292 the nearest channel point (Grieve et al., 2016).

## 293 **2.5 Landscape evolution model**

294 We use the landscape evolution model described by Litwin et al. (2024) to under-  
295 stand the sensitivity of topography and runoff generation to subsurface properties and  
296 geomorphic process rates for cases similar to those we observe at these sites. As this is  
297 a reduced complexity model intended for long-term evolution, and is initialized with small  
298 random elevation perturbations, we do not expect the model to reproduce the arrange-  
299 ment of streams and ridges at our sites. Rather we will measure key metrics of the land-  
300 scape, including hillslope length and local relief, and compare these to the site.

301 The model accounts for topographic evolution due to baselevel change, water-driven  
302 erosion using the streampower erosion equation, and hillslope sediment transport using  
303 a nonlinear hillslope diffusion equation. We decided to use a linear diffusion formulation,  
304 as the hillslopes at Baisman Run and Druids Run generally remain convex until they reach  
305 valley bottoms, and the topography shows no evidence of shallow landsliding or other  
306 mass movements. The subsurface maintains constant and spatially uniform properties  
307 through evolution, implicitly assuming that the production of permeable material keeps  
308 pace with surface erosion. The overland flow that drives fluvial erosion is generated by  
309 exfiltration and precipitation on saturated areas where the shallow aquifer reaches the  
310 land surface. The shallow aquifer model uses the Dupuit-Forcheimer assumptions to cal-  
311 culate flow over a sloping impermeable base. The aquifer receives recharge from the va-  
312 dose zone, which is represented using a single 1-dimensional profile in which discrete depth  
313 increments fill and drain by the plant-available water capacity in the increment. The pro-  
314 file dynamics are described by Schenk (2008). Evapotranspiration draws water from the  
315 shallowest available depth increment, and infiltration displaces water from the surface  
316 further into the profile. From this single profile, recharge is calculated at each aquifer  
317 node by mapping the amount of water that infiltrates into the profile below the water  
318 table depth. This one-directional coupling is computationally efficient but means that  
319 the saturated zone cannot affect vadose water storage (such as through capillary rise)  
320 or supply water for evapotranspiration. The climate is treated as a simple (Poissonian)  
321 random jump process, following Eagleson (1978), with exponentially distributed storm  
322 depth, duration, and interstorm interval, and constant evapotranspiration at the clima-  
323 tological mean rate during the interstorm periods.

324 We ran the model under the same initial and boundary conditions used in Litwin  
325 et al. (2024). The domain is square. One side boundary is fixed to baselevel, while the  
326 remaining three side boundaries are zero-flux. We began with a flat initial surface at base-  
327 level, add small random perturbations, and simulate 50 Ma of evolution until a dynamic  
328 equilibrium between erosion and uplift is reached. While this timescale is long relative  
329 to periodic changes in climate and baselevel in the Eastern Piedmont (e.g., Cleaves, 1989),  
330 we know that both sites have experienced the same forcings through their evolution, such  
331 that a single climate and baselevel change rate should still provide insights into their evo-  
332 lution.

333

## 2.6 Hydrological parameters

334

### 2.6.1 Transmissivity, hydraulic conductivity, and permeable thickness

335

336

337

338

339

340

The maximum transmissivity (hereafter just *transmissivity*) is defined as the depth-integrated saturated hydraulic conductivity. It appears in our model as the product of the effective saturated hydraulic conductivity  $k_s$  and permeable thickness  $b$ . We developed a novel method to use the saturation survey data to estimate a catchment-averaged transmissivity, building on an existing approach. We then divided that value into estimates of  $k_s$  and  $b$ .

Our method of estimating transmissivity is similar to that described by O'Loughlin (1986), as it is built on a steady state hillslope water balance and the assumption that places with the same topographic wetness index  $TI$  saturate at the same time (Beven & Kirkby, 1979). The approach begins by considering recharge that is supplied at a rate  $r(x, y)$  to the saturated zone. At hydrologic steady state, the total water outflow along a topographic contour segment with length  $v_0$  is equal to the integral of recharge over the area upslope of the contour  $A_c$ . In this way, convergent slopes will saturate before planar and divergent ones. The maximum amount of recharge that can be moved through the subsurface before saturation occurs depends on the transmissivity  $T$  and the local hydraulic gradient, which is assumed to be equal to the topographic gradient  $\nabla z$ . As a result, the criterion for saturation at the contour segment is:

$$\int_{A_c} r(x, y) dA \geq T |\nabla z| v_0. \quad (2)$$

At saturation, any additional recharge will become overland flow. Because in general the recharge is not known, O'Loughlin (1986) equated the total watershed recharge with the watershed baseflow  $Q_b$ :

$$\int_{A_{tot}} r(x, y) dA = Q_b, \quad (3)$$

where  $A_{tot}$  is the watershed area. From this expression, we derived an average recharge rate  $\bar{r} = Q_b/A_{tot}$ . Dividing Equation 2 by the average recharge rate equation and rearranging the terms, we derived an expression for the discharge-normalized transmissivity:

$$\frac{1}{|\nabla z| v_0} \int_{A_c} \left( \frac{r}{\bar{r}} \right) dA \geq \frac{T}{Q_b/A_{tot}}. \quad (4)$$

By further assuming that the integrand in the above expression is approximately unity, we obtain an expression that relates the topographic index to transmissivity and baseflow discharge:

$$\frac{A}{|\nabla z| v_0} \geq \frac{T}{Q_b/A_{tot}}. \quad (5)$$

where  $A/v_0$  is the upslope area per contour width, calculated at every point in the landscape using the digital elevation model. We will call the topographic index at boundary between saturated and unsaturated ground  $TI^*$ , which is a function of discharge  $Q_b$ . At that value the inequality in the expression above becomes equality. Using a log transform, we derived an expression for the log of transmissivity:

$$\log(T) = \log(TI^*) + \log\left(\frac{Q_b}{A_{tot}}\right). \quad (6)$$

To find  $T$  using this expression and our saturation surveys, consider a logistic regression model with the form:

$$\rho(p) = \log\left(\frac{p}{1-p}\right) = \beta_0 + \beta_1 \log\left(\frac{A}{v_0 |\nabla z|} \frac{Q_b}{A_{tot}}\right) \quad (7)$$

where  $\beta_0$  and  $\beta_1$  are parameters of the regression model. This logistic regression model is very similar to that in Equation 1, but has one fewer parameter, and consequently enforces that the odds of saturation are log-linearly dependent on the product of  $Q_b$  and

$TI$ . At the critical value of topographic index  $TI^*$ , we will call the odds of saturation  $\rho^*$ :

$$\rho^* = \beta_0 + \beta_1 \log \left( TI^* \frac{Q_b}{A_{tot}} \right). \quad (8)$$

Finally, we rearranged Equation 8 to match the form of Equation 6, and solved for the transmissivity:

$$T = e^{(\rho^* - \beta_0)/\beta_1}. \quad (9)$$

341 The main difference between this approach and that described by O’Loughlin (1986) is  
 342 that their approach equates the ratio of quickflow to precipitation with the proportion  
 343 of the watershed that is saturated, while we have direct estimates of how saturation varies  
 344 with baseflow and topographic index. This should make our approach more robust, though  
 345 it is still limited to the steady-state hydrological theory from which it was derived. Fi-  
 346 nally, we partitioned transmissivity between permeable thickness  $b$  and an effective sat-  
 347 urated hydraulic conductivity  $k_s$  based on permeable thickness values taken from the USDA  
 348 Soil Survey (Staff & Natural Resources Conservation Service, United States Department  
 349 of Agriculture., 2023) and insights gained from prior subsurface investigations of Bais-  
 350 man Run.

### 351 **2.6.2 Drainable porosity and plant available water content**

352 Drainable porosity  $n_e$  relates the depth of water stored or released when there is  
 353 a change in water table elevation. Estimates usually require either hydraulic well tests  
 354 or laboratory analyses. In the absence of hydraulic test data or permission to take soil  
 355 samples from Druids Run, we assumed that the drainable porosity was the same at both  
 356 sites. Plant available water content ( $n_a$ ) is the amount of water available for plant use  
 357 per unit volume of soil. The values were estimated based on the USDA Soil Survey data  
 358 for the dominant soil types at the two sites.

### 359 **2.6.3 Climatological parameters**

We fit three independent exponential distributions for storm depth  $d_s$ , duration  $t_r$ ,  
 and interstorm duration  $t_b$  by calculating the mean values of these quantities from a pre-  
 cipitation dataset previously collected from 2014-2018 at the weather station at Bais-  
 man Run (Cosans, 2022). Because the two sites are very close together, this one time-  
 series was used to calculate storm statistics at both sites. The distributions are:

$$f(d_s) = \frac{1}{\langle d_s \rangle} \exp \left( - \frac{d_s}{\langle d_s \rangle} \right) \quad (10)$$

$$f(t_r) = \frac{1}{\langle t_r \rangle} \exp \left( - \frac{t_r}{\langle t_r \rangle} \right) \quad (11)$$

$$f(t_b) = \frac{1}{\langle t_b \rangle} \exp \left( - \frac{t_b}{\langle t_b \rangle} \right) \quad (12)$$

$$(13)$$

360 where the angled braces indicate the temporal mean of the quantity. Potential evapo-  
 361 transpiration (ET) was estimated based on the average annual value in Baltimore be-  
 362 tween 1981 and 2010, as reported by the Northeast Regional Climate Center at Cornell  
 363 University. In our model, ET only occurs during interstorm periods, so the interstorm  
 364 potential ET rate  $pet$  was estimated by rescaling the average potential ET rate with the  
 365 interstorm time fraction. Our climatological approach is simplistic, neglecting covariance  
 366 of storm depth, duration, and interstorm duration, seasonality, paleoclimatic variabil-  
 367 ity, and so on. However, we do not expect any large differences in the climate between  
 368 the two sites, so even a simple approach should allow us to make comparisons of how land-  
 369 scapes with different geomorphic and subsurface hydrologic properties respond to climatic  
 370 conditions similar to those observed at our sites.

## 371 2.7 Estimating geomorphic parameters

372 The topographic parameters of our model are the uplift or baselevel change rate  
 373  $U$ , hillslope diffusivity  $D$ , streampower incision coefficient  $K$ , characteristic contour width  
 374  $v_0$ , and the streampower exponents  $m$  and  $n$ , as discussed below. The Piedmont is thought  
 375 to reasonably approximate geomorphic steady state (Pavich, 1989; Bazilevskaya et al.,  
 376 2013), so we set the rate of baselevel fall equal to the average cosmogenic  $^{10}\text{Be}$  erosion  
 377 rate from nearby Piedmont sites. The remaining parameters were identified using topo-  
 378 graphic analysis. The methods presented below are largely consistent with methods used  
 379 by others in the literature, except for the streampower parameters. There we present a  
 380 modification of a previously-proposed method, adapted to account for the effect of hy-  
 381 drologic variability.

### 382 2.7.1 Hillslope diffusivity

Hillslope diffusivity can be derived from the rate of baselevel change  $U$  and hill-  
 top curvature  $C_{HT}$  (Roering et al., 2007; Hurst et al., 2012):

$$D = -\frac{U}{C_{HT}}. \quad (14)$$

383 In hillslope evolution contexts, it is typical to account for the ratio of the bulk densities  
 384 of regolith (on which the diffusion process occurs) and parent material (on which base-  
 385 level change occurs) (Roering et al., 2007). Because we are working with an integrated  
 386 channel and hillslope model, and we do not have good estimates for the bulk density of  
 387 fluviually-eroded material, we will neglect the bulk density terms. In this context,  $D$  is  
 388 an effective diffusivity that will match the simulated hilltop curvature with that from  
 389 our topographic measurements. We calculated the hilltop curvature by taking the sec-  
 390 ond derivative of a polynomial surface fit to a 10 m footprint around each hilltop point.  
 391 Hilltop points are the same as those used for the hillslope length analysis. The footprint  
 392 size was selected by calculating the hilltop curvature for footprints of varying sizes and  
 393 selecting the size at which there is a break in the standard deviation of curvature, fol-  
 394 lowing the procedure described by Hurst et al. (2012).

### 395 2.7.2 Streampower parameters

We estimated the streampower law parameters using an integral approach called  
 $\chi$ -analysis (Perron & Royden, 2013). While the parameters can be derived from slope-  
 area analysis, slope estimates often have significant noise that can result in poor param-  
 eter estimates (Perron & Royden, 2013). The integral approach is more stable, as it only  
 requires the elevation and the upslope area to calculate the model parameters. The typ-  
 ical  $\chi$ -analysis needed slight modification to accommodate our landscape evolution model.  
 Litwin et al. (2022) derived the fluvial incision term of the landscape evolution model  
 with assumptions that yielded linear dependence on the dimensionless discharge  $Q^*$ , a  
 slope exponent  $n = 1$ , and area exponent  $m = 1/2$ . We derived a more general form  
 by assuming that the exponent that determines the channel width from area and the ex-  
 ponent that determines erosion rate from shear stress were free parameters:

$$E_f = KQ^{*n} (v_0a)^m |\nabla z|^n \quad (15)$$

where  $E_f$  is the fluvial incision rate,  $K$  is the erodibility,  $v_0$  is the characteristic contour  
 width,  $a$  is the area per contour width, and  $\nabla z$  is the elevation gradient. For simplic-  
 ity, we will use the variable  $Q^*$  to refer to the temporally-averaged dimensionless discharge  
 which is called  $\langle Q^* \rangle$  in Litwin et al. (2024). Because  $\chi$ -analysis is usually only applied  
 to river channels, it is typical to neglect the hillslope diffusion term, and write the so-  
 lution at equilibrium between uplift and fluvial incision along a channel distance coor-  
 dinate  $x$ :

$$U = KQ^{*n} (v_0a)^m \left| \frac{\partial z}{\partial x} \right|^n. \quad (16)$$

We then solved for  $|\partial z/\partial x|$ , and substituted area for area per contour width times the characteristic contour width  $A = v_0 a$ :

$$\left| \frac{\partial z}{\partial x} \right| = \left( \frac{U}{KQ^{*n}} \right)^{1/n} A^{-m/n}. \quad (17)$$

Next we normalized upslope area to a reference drainage area  $A_0$ , and integrated the equation above with respect to  $x$ :

$$z(x) = z(x_b) + \int_{x_b}^x \left( \frac{U}{KQ^{*n}A_0^m} \right)^{1/n} \left( \frac{A_0}{A(x)} \right)^{m/n} dx \quad (18)$$

where  $z(x_b)$  is the elevation at a specified baselevel location  $x_b$ . In general,  $Q^*$  varies with position, so we cannot remove it from the integral. However, in our model  $Q^*$  generally approaches a constant value as you move downstream equal to one minus the actual evapotranspiration relative to precipitation  $1 - \langle AET \rangle / \langle P \rangle$ , which is approximately the mean runoff ratio  $\langle Q \rangle / \langle P \rangle$ . We will call this value  $Q_{max}^*$ . Then we can write:

$$z(x) = z(x_b) + \left( \frac{U}{KQ_{max}^{*n}A_0^m} \right)^{1/n} \chi, \quad (19)$$

where

$$\chi = \int_{x_b}^x \left( \frac{A(x)}{A_0} \right)^{m/n} dx. \quad (20)$$

These equations show that the elevation of a stream channel in dynamic equilibrium should be linear with respect to  $\chi$  if  $U$ ,  $K$ , and  $Q_{max}^*$  are uniform, and that the slope of that relationship should be:

$$k_{sn} = \left( \frac{U}{KQ_{max}^{*n}A_0^m} \right)^{1/n}, \quad (21)$$

396 which is often called the normalized channel steepness index. Note that this is related  
397 to but distinct from our use of “steepness” in Litwin et al. (2022).

We calculated the slopes of channel segments in  $\chi$ -elevation space for the channel networks we extracted previously. Because the reference drainage area  $A_0$  is introduced for dimensional purposes only, we can set it equal to unity, and solve for the streampower incision coefficient  $K$ :

$$K = \frac{U}{(k_{sn}Q_{max}^*)^n}. \quad (22)$$

## 398 **3 Results**

### 399 **3.1 Hydrologic and geomorphic observations**

#### 400 **3.1.1 Discharge, baseflow, and runoff ratio**

401 Figure 3 shows the timeseries of discharge and precipitation for both sites. Base-  
402 flow (in dark blue) at Baisman Run declined from early summer continuing until Octo-  
403 ber, when a small persistent increase is combined with episodic increases in response to  
404 large storms. Unfortunately the discharge timeseries available to us at Druids Run is too  
405 short to look at annual trends, though there does appear to be a significant baseflow de-  
406 cline from spring into summer, leading to low flows by late June. We did not observe no-  
407 flow conditions at the gage location, but we do know that flows were often close to or  
408 below the pressure transducer detection limit during the summer.

409 The storm runoff ratio is substantially more variable at Druids Run than Baisman  
410 Run. We identified 21 storm events at Druids Run and 43 storm events at Baisman Run,  
411 and found that the total event precipitation explained most of the variation in total event  
412 quickflow  $Q_{f,event}$  (Figure 4). Events are colored by the antecedent baseflow, which shows

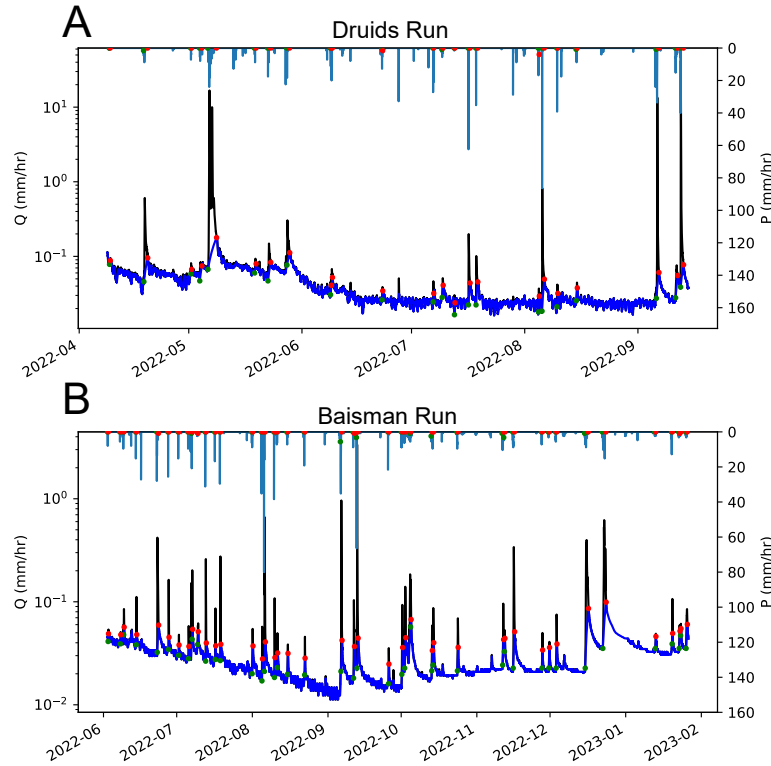


**Figure 3.** Timeseries of discharge  $Q$  (black), baseflow  $Q_b$  (dark blue), and precipitation  $P$  (light blue) at Druids Run (A) and Baisman Run (B). Storm events that we identified based upon the baseflow separation and precipitation begin with green dots and end with red dots, which are placed at the corresponding times on both the precipitation and discharge timeseries. Note that the timeseries for Baisman Run and Druids Run are not aligned in time.

413 that some of the variation in event runoff that cannot be explained by event precipita-  
 414 tion may be explained by antecedent conditions. To quantify the sensitivity of event runoff  
 415 to event precipitation, we fit the curve  $Q_{f,event} = a_2 P_{event}^{a_1}$ , where the log-space slope  
 416 corresponds to the fitted exponent  $a_1$ . The exponent and standard error are  $3.17 \pm 0.40$   
 417 and  $1.89 \pm 0.13$  at Druid Run and Baisman Run, respectively. An exponent  $a_1 = 1$  would  
 418 indicate that the storm runoff is a constant proportion of the event precipitation. When  
 419 the event runoff ratio is interpreted as the effective proportion of the watershed contribut-  
 420 ing runoff (O’Loughlin, 1986), an exponent closer to one indicates that the contribut-  
 421 ing area does not vary with storm size. This interpretation suggests that contributing  
 422 areas vary with precipitation at both sites, but they are more variable at Druids Run  
 423 than Baisman Run. This interpretation also suggests that as storm events approach 100  
 424 mm, nearly all of Druids Run contributes storm runoff (4A). These events are fairly fre-  
 425 quent; the annual maximum recurrence interval of 100 mm of precipitation in 24 hours  
 426 is approximately two years at our sites (NOAA, 2024).

### 427 3.1.2 Saturated areas

428 At Druids Run, observed saturation was highly variable in time and correlated with  
 429 discharge. We measured saturation five times along nine transects, seven of which run  
 430 along first order drainages or the interfluves between them, and two of which run par-

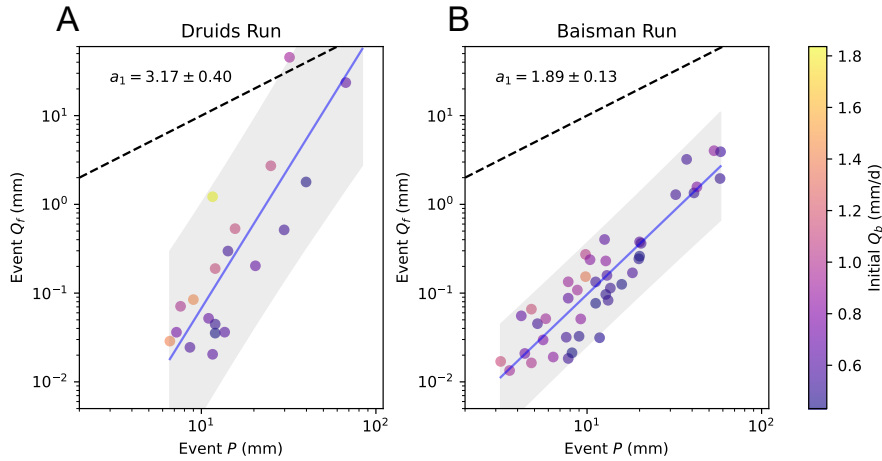


**Figure 4.** Event runoff characteristics for Druids Run (A) and Baisman Run (B). Event totals are calculated by summing the 15-minute precipitation and quickflow timeseries over the event durations. The points are colored by the initial baseflow  $Q_b$ . The dotted line is a 1:1 line, which represents the case where event runoff is equal to event precipitation. The blue line is a power law regression with the form  $Q_{f,event} = a_2 P_{event}^{a_1}$ , and the shaded area is the 95% confidence interval on the regression. The range on the coefficient  $a_1$  is given as the standard error.

431 allel to the valley bottom (Figure 5A–E). The surveys conducted under the two high-  
 432 est flow conditions (C, E) had the greatest number of saturated points. Saturation was  
 433 often discontinuous with distance downstream in first order channels. Upslope areas some-  
 434 times saturated and flowed first, while downslope reaches remained dry, as flow passed  
 435 through the subsurface. First order channels tend to have exposed bedrock or thin al-  
 436 luvial cover near their headwaters, while closer to the valley bottom they become sub-  
 437 merged in alluvium that has sufficient capacity to move the water from upslope through  
 438 the subsurface. Bedrock fractures may also play a role in redistributing surface flow to  
 439 subsurface pathways.

440 In contrast, saturated areas were more persistent at Baisman Run. We measured  
 441 saturation four times along six transects, four of which run perpendicular to the valley  
 442 bottom, and two run parallel to it (Figure 5F–I). Regardless of discharge, we found that  
 443 saturation was confined to locations at or below the distinct break in slope where the  
 444 hillslopes meet the valley bottom. Within the valley bottom, saturation was not present  
 445 everywhere, as the stream channel is incised into the valley bottom alluvium in some places.  
 446 Flow emerges at distinct springs and seeps at the break in slope (Putnam, 2018). The  
 447 springs are further evidence that subsurface pathways support baseflow, while the rel-  
 448 atively persistent nature of saturated areas support our observation that event quick-  
 449 flow is less sensitive to event precipitation at Baisman Run than it is at Druids Run.

450 We used the logistic model (Equation 1) to predict the odds of saturation for the  
 451 range of topographic index values in each watershed and the range of discharge values  
 452 at which saturation surveys were conducted (Figure 6). The parameters of the fitted model  
 453 are shown in Table 1. In Figure 6, the topographic index value at which the black dashed  
 454 line intersects the odds ratio curves is the critical value of  $TI$  where saturation becomes  
 455 more likely than not for a given value of discharge. We plotted this together with the  
 456 probability density of watershed topographic index (orange) to show how the critical  $TI$   
 457 relates to the distribution of  $TI$  for the watershed.



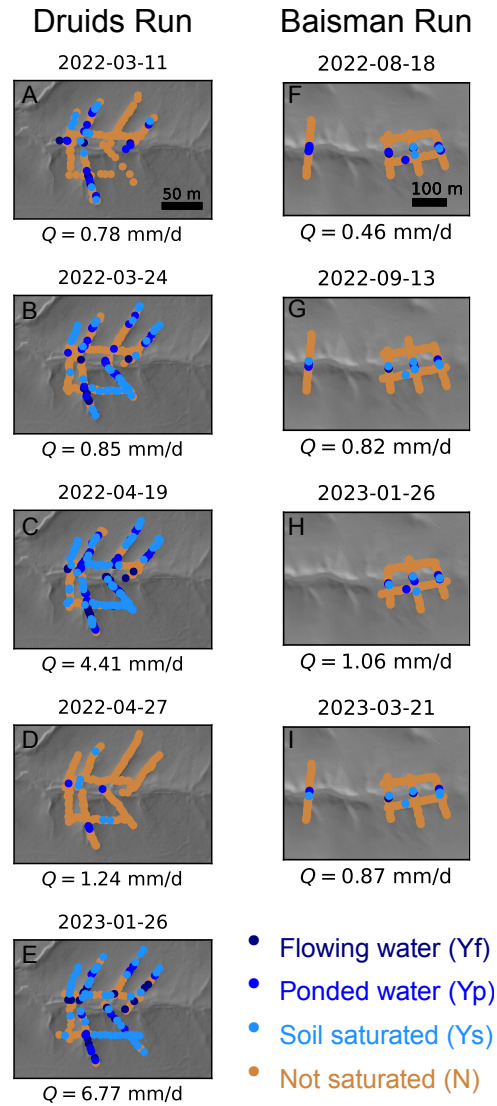


**Figure 5.** Observations of saturation made on transects at Druids Run (A–E) and Baisman Run (F–I). The latter plots have been rotated 90 degrees such that north is in the direction of the positive x-axis. In both figures, flow in the valley bottom is from right to left. The classification and sampling approaches are described in Section 2.2.

	$\alpha_0$	$\alpha_1$	$\alpha_2$
Druids Run	$4.609 \pm 0.637$	$0.174 \pm 0.040$	$1.000 \pm 0.097$
Baisman Run	$-7.559 \pm 4.299$	$0.703 \pm 0.103$	$0.070 \pm 0.590$

**Table 1.** Estimated parameter values of the logistic regression models for saturation (Equation 1), where  $\alpha_0$  is the intercept,  $\alpha_1$  is the coefficient on topographic index, and  $\alpha_2$  is the coefficient on the area-normalized discharge. Parameter ranges are given as standard errors.

458 The regression model for Druids Run in Figure 6A shows that the predicted odds  
 459 of saturation varies substantially with discharge. When discharge is small, the critical  
 460  $TI$  value confines likely saturation to a very small portion of the total watershed area,  
 461 while for large discharge the critical value of  $TI$  is low enough that most of the water-  
 462 shed is likely to be saturated. This supports the high variability of saturation in space  
 463 and time that we inferred from the pointwise measurements.

464 The logistic regression model predicts very different behavior for Baisman Run (Fig-  
 465 ure 6B). First, we notice that the saturation odds curve does not vary with discharge,  
 466 such that all curves overlap. This is reflected in the regression parameter  $\alpha_2$  on dis-  
 467 charge (Table 1), which is much smaller and more uncertain for Baisman Run than Druids  
 468 Run. As a result, the critical value of topographic index is nearly constant with time.  
 469 Second, we notice that the curves are narrower and steeper than those estimated for Druids  
 470 Run, such that the odds of saturation increases more abruptly around the critical value  
 471 of  $TI$ . This is reflected in the regression parameter  $\alpha_1$  on topographic index, which is  
 472 much larger at Baisman Run than Druids Run. This supports our observation that sat-  
 473 uration emerges abruptly at the transition from hillslopes to valley bottoms.

474 The logistic regression models also allowed us to generalize the saturation predic-  
 475 tions to the entire watersheds. We predicted saturation through time for the discharge  
 476 timeseries in Figure 3 and for all raster points based upon their topographic index. We  
 477 then classified whether each point was “wet” (exceeded criteria for saturation greater than  
 478 95% of the time), “dry” (exceeded criteria for saturation less than 5% of the time), or  
 479 variably saturated if it met neither of those criteria.

480 Figure 7 shows a dramatic difference in the hydrological function of the two sites  
 481 based on the logistic regression model predictions. The predicted channel network at Druids  
 482 Run was ephemeral until close to the watershed outlet. Variable saturation is widespread  
 483 in zero-order basins and onto some hilltops, but as Figure 6A shows, saturation at these  
 484 locations with low topographic index only occurs at the high discharge values, which are  
 485 associated with storm events. Some of the hillslopes we sampled that appear as “dry”  
 486 may in fact saturate occasionally, but less than 5% of the time. In contrast, the regres-  
 487 sion model predicted that Baisman Run had a continually wet stream channel over the  
 488 course of our observation period, and did not experience saturation on the hillslopes.

489 Analysis of rainfall-runoff and saturation data reveal the dramatic difference be-  
 490 tween hydrological function of the two sites. When the permeable subsurface is thin, as  
 491 at Druids Run, much of the landscape saturates and desaturates relatively easily in re-  
 492 sponse to precipitation, and the effective proportion of the watershed contributing runoff  
 493 varies substantially. In contrast, when the permeable subsurface is thick, as at Baisman  
 494 Run, the same precipitation causes modest or no change in saturated areas, though new  
 495 subsurface flow paths may still be activated with increasing storm size, such that the ef-  
 496 fective contributing area increases with increasing wetness.

497 The dynamics of saturated areas with discharge can be considered an extension of  
 498 work on flowing channel length dynamics (e.g., Prancevic & Kirchner, 2019). Our results

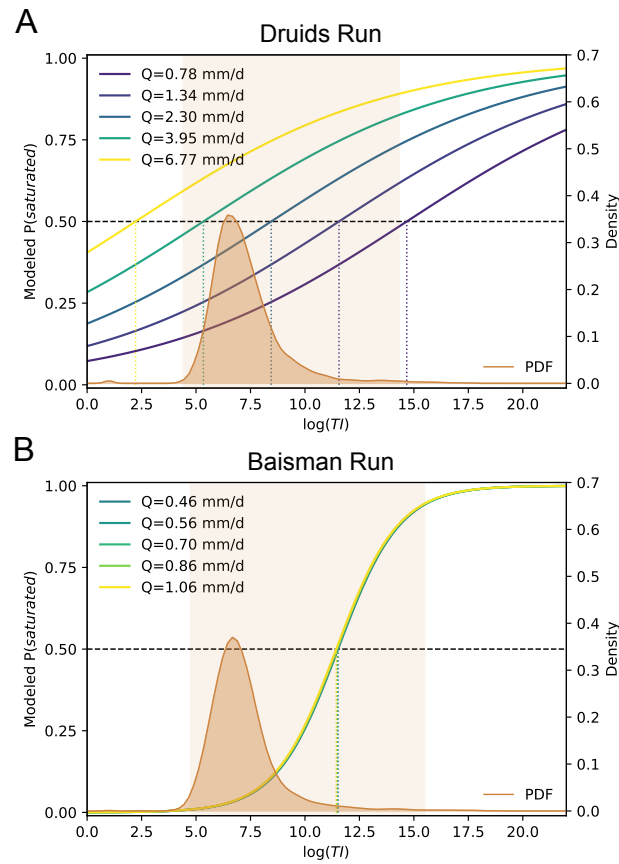


**Figure 6.** Regression results for Druids Run (A) and Baisman Run (B). The regression model has the form given in Equation 1. The modeled probability of saturation is given in terms of topographic index and discharge, where discharge varies logarithmically across the range of saturation survey discharge values. There is a dashed line at the 50% probability mark, and where this intersects each one of the probability curves, there is a dotted line dropped to the x-axis. This indicates the critical value of topographic index at which saturation is more likely than not to occur given that value of discharge. On the opposing axis is the probability density of topographic index, estimated with a kernel density approach. The lighter shaded region indicates the range of  $TI$  values sampled in our surveys, which indicates good topographic index coverage of our samples.

499 also show that the dynamics of saturation depend on a balance of upslope water sup-  
 500 ply and downslope transport capacity, which can be related to subsurface properties and  
 501 topography.

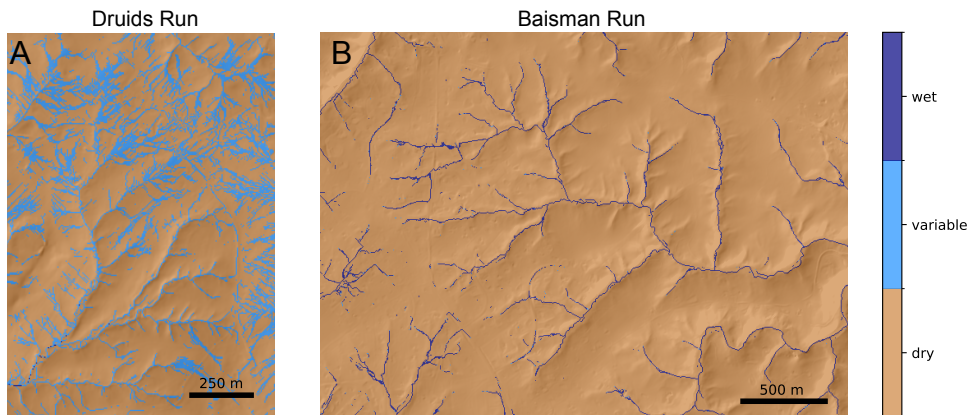


**Figure 7.** Classified saturated areas for Druids Run (A) and Baisman Run (B), based on the logistic regression model in Equation 1 and shown in Figure 6, and the runoff timeseries shown in Figure 3. The modeled probability necessary for saturation was set at 50%. A location was classified as “wet” if it exceeded criteria for saturation greater than 95% of the time, “dry” if it exceeded criteria for saturation less than 5% of the time, or variably saturated if it was in between.

### 502 *3.1.3 Hillslope length and relief*

503 Both hillslope length and relief are greater at Baisman Run than Druids Run. The  
 504 channel networks and hilltop points from which hillslope length and relief were defined  
 505 are shown in Figure 2. Totals of  $5.3 \times 10^4$  and  $7.0 \times 10^4$  hilltop points with unique length  
 506 and relief were identified at Druids Run and Baisman Run, respectively. The median hill-  
 507 slope length is 88.3 m at Druids Run and 177.3 m at Baisman Run, while median relief  
 508 was 2.9 m at Druids Run and 6.7 m at Baisman Run. In trying several other channel  
 509 network extraction methods, we found that the hillslope length distributions varied but  
 510 that hillslopes were still generally shorter at Druids Run than Baisman Run. Figure 8A  
 511 shows that there is no overlap in the interquartile range (IQR) of hillslope length or re-  
 512 lief for the two sites. The strength and sign of this difference supports our hypothesis  
 513 that the site with a thick permeable subsurface will have greater hillslope length and re-  
 514 lief than that with a thin permeable subsurface.

### 515 **3.2 Landscape evolution parameterization**

516 While both the hydrological and geomorphic differences between Druids Run and  
 517 Baisman Run support our hypotheses, we have not yet established that the subsurface  
 518 is the link between the emergent hydrological function and morphology. To do so, we es-  
 519 timated the parameters for DupuitLEM, and ran the model under conditions that ap-  
 520 proximate those found at our sites. Using the approaches described in Sections 2.6 and  
 521 2.7, we estimated all the parameters needed to run the model without calibration. Pa-  
 522 rameters are estimated independently from one another, though we assume that both  
 523 sites have experienced the same uplift rate  $U$ .

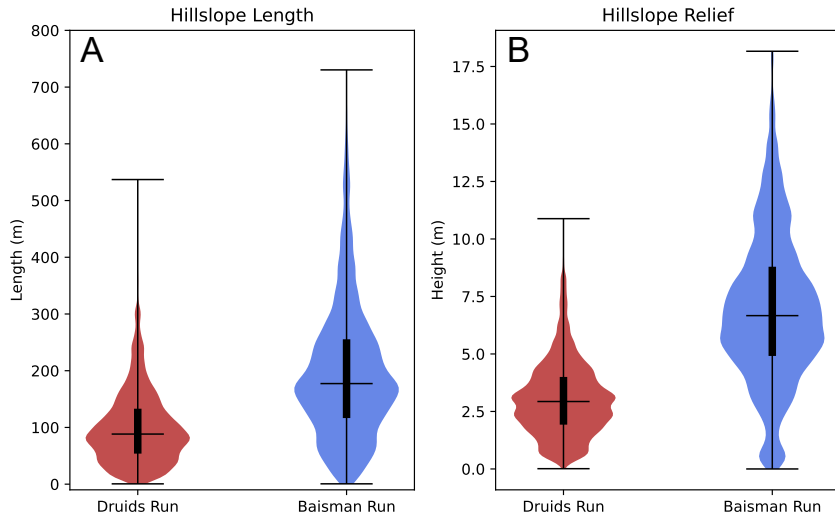


**Figure 8.** Violin plots of hillslope length and relief for Druids Run (A) and Baisman Run (B). Hillslope length is the length along a flow path from a hilltop point to the nearest channel point along a flowpath. Hillslope relief is the drop in elevation over that distance. Violin plots show the median, minimum, and maximum (horizontal lines) values and the interquartile range (wider vertical bar).

524

### 3.2.1 Hydrologic parameters

525

526

527

528

529

530

531

532

533

534

535

536

537

538

539

540

541

542

543

544

545

546

547

548

We first estimated the transmissivity using Equation 9. We estimated the parameters  $\beta_0$  and  $\beta_1$  by fitting Equation 7 using topographic index, discharge, and saturation survey data. With the fitted model, we determined the optimal threshold probability  $p^*$  at which saturation was likely to occur. While we could have chosen 50% as we did in the regression model for saturated area, we found that this performed poorly on the simpler two-parameter formulation used to calculate transmissivity. The selected value of  $p^*$  should balance correctly classifying points as saturated (high true positive ratio (TPR)) and minimizing the number of points that are misclassified as saturated (low false positive ratio (FPR)). Plotting TPR against FPR gives the receiver operating characteristic curve, from which we selected the optimal threshold probability by maximizing the difference TPR-FPR. The results of this process are shown in Figure 9. Using the optimal  $p^*$ , we estimated the transmissivity from Equation 9 10,000 times using Monte Carlo simulations to determine the uncertainty due to the variance and covariance of the logistic regression parameters. The median and quartiles of transmissivity are reported in Table 2. This approach predicts that the transmissivity at Baisman Run is nearly 3.5 times higher than at Druids Run. There is no overlap between the IQRs of the estimated transmissivities, which suggests a robust difference between the two sites. The uncertainty we have quantified reflects that of the regression parameters, but does not include the optimal threshold predicted by maximizing TPR-FPR. The ambiguity in the peak value (Figure 9D) suggests that transmissivity and its uncertainty may be larger than we have predicted. There is also uncertainty related to methodological choices (raster resolution, flow routing method, threshold selection method), but experimentation suggested that the median transmissivity is always larger at Baisman Run than Druids Run when the same methodology is applied to both sites.

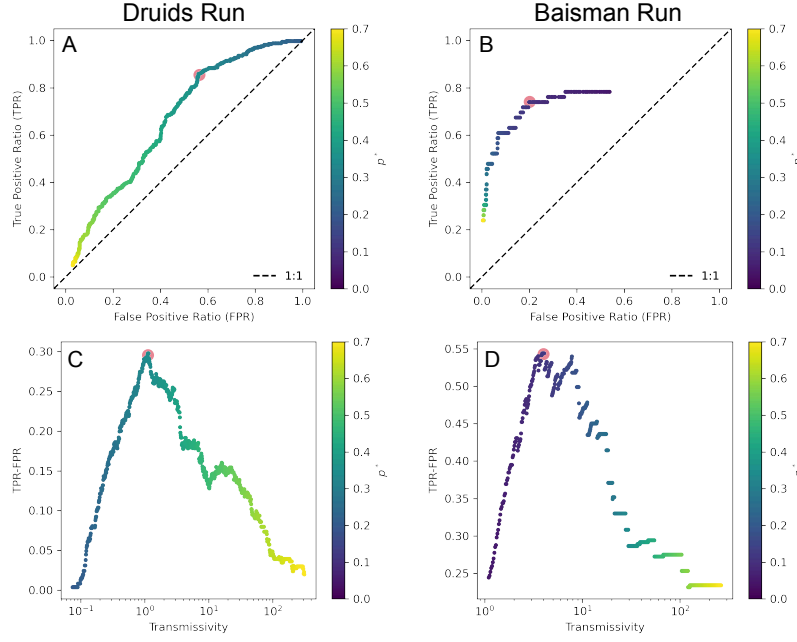


**Figure 9.** Results of the TPR-FPR analysis. (A–B) The receiver operating characteristic curve for Druids Run and Baisman Run, respectively, colored by the threshold value  $p^*$  used to obtain each combination of quantities. (C–D) The difference TPR-FPR, which we seek to maximize, plotted against the transmissivity value associated with each threshold  $p^*$ . We selected the transmissivity associated with the largest value of TPR-FPR.

	Transmissivity ( $\text{m}^2/\text{d}$ )			Regression Parameters			
	Med	LQ	UQ	$\bar{\beta}_0$	$\bar{\beta}_1$	$\rho^*$	$p^*$
Druids Run	1.12	0.88	1.40	-0.691	0.268	-0.660	0.341
Baisman Run	3.89	3.24	4.64	-3.012	0.693	-2.072	0.112

**Table 2.** Median (Med), lower and upper quartiles (LQ, UQ) of transmissivity estimated from the logistic regression model, and the associated regression model parameters. The bar over a variable indicates the mean value.

549 To estimate the effective hydraulic conductivity from transmissivity, we first esti-  
 550 mated the permeable thickness. At Druids Run, data from the USDA Soil Survey sug-  
 551 gested a strong permeability contrast at the base of the A horizon, so we used the char-  
 552 acteristic A horizon thickness as our permeable thickness (Staff & Natural Resources Con-  
 553 servation Service, United States Department of Agriculture., 2023). At Baisman Run,  
 554 there is no strong permeability contrast within the soil profile, so we used the entire soil  
 555 profile thickness, weighted for the different soil types found in the watershed (2.03 m).  
 556 We added 2 m to this value to approximate the average saprolite thickness between ridges  
 557 and valleys in Baisman Run (Cosans, 2022). Our model is generally less sensitive to thick-  
 558 ness than to maximum transmissivity, so we do not expect the results to be highly sen-  
 559 sitive to the possible range of this value (Litwin et al., 2022, 2024). We divided trans-  
 560 missivity by the permeable thickness, and found that the effective hydraulic conductiv-  
 561 ity is in fact larger at Druids Run ( $2.84 \times 10^{-5}$  and  $1.12 \times 10^{-5}$  for Druids Run and

562 Baisman Run, respectively), suggesting the difference in thickness accommodates the dif-  
 563 ference in transmissivity. The values are shown in Table 3.

564 We estimated drainable porosity and plant-available water content from literature  
 565 values. We assumed drainable porosity was constant and equal to 0.25 at both sites, which  
 566 is typical for materials with medium sand to medium gravel texture (Johnson, 1967). While  
 567 drainable porosity is an important variable for regulating the degree to which the wa-  
 568 ter table rises and falls in response to recharge, it has a relatively narrow range of pos-  
 569 sible values in comparison to other parameters, so a possible difference between the sites  
 570 should not have a strong effect on our results. We estimated plant-available water con-  
 571 tent as 0.19 and 0.14 for Druids Run and Baisman Run respectively using characteris-  
 572 tic values for our sites from the USDA Soil Survey.

573 Lastly, climatological variables were estimated using the approaches described in  
 574 the methods section with weather station data and literature values. The relevant val-  
 575 ues are shown in Table 3.

Name	Symbol	Units	Druids Run	Baisman Run
Hydraulic conductivity	$k_s$	m/s	2.84e-5	1.12e-5
Permeable thickness	$b$	m	0.46	4.03
Plant-available water content	$n_a$	-	0.19	0.14
Drainable porosity	$n_e$	-	0.25	0.25
Mean storm duration	$\langle t_r \rangle$	s	1.02e4	1.02e4
Mean interstorm duration	$\langle t_b \rangle$	s	1.11e5	1.11e5
Mean storm depth	$\langle d_s \rangle$	m	4.50e-3	4.50e-3
Interstorm potential ET rate	$pet$	m/s	2.58e-8	2.58e-8

**Table 3.** All hydrological parameters needed to run DupuitLEM. The values for  $n_e$ ,  $\langle t_r \rangle$ ,  $\langle t_b \rangle$ ,  $\langle d_s \rangle$ , and  $pet$  are identical at the two sites.

### 576 3.2.2 Geomorphic parameters

577 The uplift or baselevel change rate  $U$  is an important model parameter and is needed  
 578 to obtain estimates of both the hillslope diffusivity  $D$  and the streampower incision co-  
 579 efficient  $K$ . Portenga et al. (2019) estimated the mean denudation rate of the Piedmont  
 580 in the nearby Potomac River basin as 11.4 m/Myr (IQR 7.6 – 15.0) assuming an aver-  
 581 age rock density of 2700 kg/m<sup>3</sup>. We equated the denudation rate with uplift rate  $U$ , as-  
 582 suming geomorphic steady state. To quantify the uncertainty in  $U$ , and its contribution  
 583 to the uncertainty in  $D$  and  $K$ , we estimated a probability distribution for  $U$  based on  
 584 the box plot in Figure 4 of Portenga et al. (2019). The data did not appear particularly  
 585 skewed, so we modeled denudation with a normal distribution, which we truncated to  
 586 permit only positive values.

587 We estimated the diffusivity based on hilltop curvature, as presented in Equation  
 588 14. All the parameter values needed are shown in Table 4, and the distributions of the  
 589 log of hilltop curvature are shown in Figure 10A. Hilltop curvature is quite similar at both  
 590 sites. This is surprising because different processes likely contribute to diffusive trans-  
 591 port at Druids Run versus Baisman Run. For example, freeze-thaw effects may be more  
 592 important in the exposed, rocky soils at Druids Run, while treethrow may be more im-  
 593 portant in the forest-covered soils at Baisman Run. We estimated the diffusivity and its  
 594 uncertainty by Monte Carlo simulation, sampling the distribution of  $U$  10,000 times, and  
 595 selecting 10,000 values from the hilltop curvature dataset independently with replace-  
 596 ment. The distributions of diffusivity from the Monte Carlo simulation are shown in Fig-

597 ure 10B. The median diffusivity is  $8.6\text{e-}3 \text{ m}^2/\text{yr}$  (IQR  $4.4\text{e-}3 - 1.7\text{e-}2$ ) at Druids Run,  
 598 and  $9.3\text{e-}3 \text{ m}^2/\text{yr}$  (IQR  $4.3\text{e-}3 - 1.9\text{e-}2$ ) at Baisman Run.

	$C_{HT} \text{ (m}^{-1}\text{)}$			$U \text{ (m/yr)}$		
	Med	LQ	UQ	Med	LQ	UQ
Druids Run	$-1.272\text{e-}3$	$-2.084\text{e-}3$	$-7.053\text{e-}4$	$1.193\text{e-}5$	$7.561\text{e-}6$	$1.495\text{e-}5$
Baisman Run	$-1.125\text{e-}3$	$-2.123\text{e-}3$	$-6.571\text{e-}4$	$1.193\text{e-}5$	$7.561\text{e-}6$	$1.495\text{e-}5$

**Table 4.** Hilltop curvature  $C_{HT}$  and uplift  $U$  for Baisman Run and Druids Run. Negative curvature indicates convexity. Uplift values are the same for both sites.

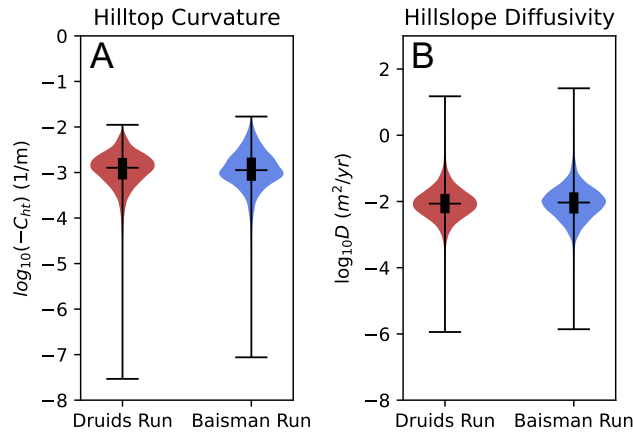


**Figure 10.** Violin plots of the log of hilltop curvature and log of hillslope diffusivity for Druids Run (A) and Baisman Run (B). Violin plots show the median, minimum, and maximum (horizontal lines) values and the interquartile range (wider vertical bar). Both distributions are similar, though Druids Run has slightly higher curvature, and therefore slightly lower diffusivity.

599 We calculated the streampower incision coefficient  $K$  using Equation 22 by esti-  
 600 mating  $n$ ,  $k_{sn}$ , and  $Q_{max}^*$ . We first conducted a  $\chi$ -analysis of the channel networks of  
 601 both sites to determine the streampower exponent  $n$  and then the appropriate steepness  
 602 index  $k_{sn}$ . Lastly, we estimated the maximum dimensionless discharge  $Q_{max}^*$  based on  
 603 available hydrologic data.

604 To calculate the optimal coordinate  $\chi$ , we need to estimate the concavity index  $m/n$   
 605 (see Equation 20) for which the channel network collapses to a single line in  $\chi$ -elevation  
 606 space (Perron & Royden, 2013). We tried a range of values for the concavity index and  
 607 determined that  $m/n = 1/2$  produced a satisfactory collinearity of channels for both  
 608 of the sites. Independently estimating the exponents  $m$  and  $n$  is challenging (Harel et  
 609 al., 2016), so we chose the combination  $m = 1/2$  and  $n = 1$  for consistency with our  
 610 prior modeling studies.

611 We determined  $k_{sn}$  from the slope of the relationship between  $\chi$  and elevation for  
 612 individual channel segments using the method described by S. M. Mudd et al. (2014).  
 613 We estimated  $K$  using the segments that are above the 40<sup>th</sup> percentile of channel net-  
 614 work drainage area, which are colored by  $k_{sn}$  in Figure 11A–B. We selected this drainage



615 area cutoff to isolate channel segments where  $Q^*$  is less likely to vary with distance down-  
 616 stream. We found that channel segments with smaller upslope areas were often less lin-  
 617 ear in  $\chi$ -elevation space, which may indicate a change in  $Q^*$  with area. Figure 11C shows  
 618 the distribution of  $k_{sn}$  values that meet these criteria. We found that  $k_{sn}$  was nearly twice  
 619 as high at Druids Run, with a median of 2.774 (IQR 2.163 – 3.284), as Baisman Run,  
 620 with a median of 5.23 (IQR 4.747 – 7.017).

	$k_{sn}$ (m)			Exponents (-)		Runoff (-)
	Median	LQ	UQ	$m$	$n$	$Q_{max}^*$
Druids Run	2.774	2.163	3.284	0.5	1	0.3
Baisman Run	5.230	4.747	7.017	0.5	1	0.3

**Table 5.** Channel steepness index  $k_{sn}$ , streampower exponents, and maximum runoff rate  $Q_{max}^*$  for Baisman Run and Druids Run.

621 We estimated the maximum dimensionless discharge  $Q_{max}^*$  at Baisman Run as the  
 622 long-term average runoff ratio  $\langle Q \rangle / \langle P \rangle = 0.3$  (Cosans, 2022). From our short timeseries  
 623 at Druids Run, we calculated a runoff ratio of 0.57. Because  $k_{sn}$  depends on the prod-  
 624 uct of  $K$  and  $Q_{max}^*$  (Equation 21) in our model, these data suggest that the factor of  
 625 two difference in  $k_{sn}$  between our sites could be due to the difference in the hydrology,  
 626 expressed in  $Q_{max}^*$ , rather than a difference in material and geomorphic properties, ex-  
 627 pressed in  $K$ . While that would support our hypothesis, we will conservatively set  $Q_{max}^* =$   
 628 0.3 for Druids Run as a first estimate, matching Baisman Run.

629 With all components of Equation 22 estimated, we used the same Monte Carlo pro-  
 630 cedure to calculate  $K$  and its uncertainty. Figure 11D shows that  $K$  is substantially higher  
 631 at Druids Run than at Baisman Run when  $Q_{max}^*$  is set equal. The median at Druids Run  
 632 is  $1.34e-5 \text{ yr}^{-1}$  (IQR  $8.24e-6 - 1.98e-5$ ), while at Baisman Run it is  $6.49e-6 \text{ yr}^{-1}$  (IQR  
 633  $3.83e-6 - 9.66e-6$ ). The full table of geomorphic parameters are shown in Table 6.

Name	Symbol	Units	Druids Run	Baisman Run
Uplift rate	$U$	m/yr	$1.143e-5$	$1.143e-5$
Hillslope diffusivity	$D$	$\text{m}^2/\text{yr}$	$8.611e-3$	$9.285e-3$
Streampower incision coefficient	$K$	1/yr	$1.334e-5$	$6.546e-6$
Contour length	$v_0$	m	30	30

**Table 6.** Geomorphic parameters needed to run DupuitLEM. We used the median value from the estimated parameter distributions for  $U$ ,  $D$ , and  $K$ . The values for  $U$  and the characteristic contour length  $v_0$  are identical at the two sites.

634 The difference in streampower incision coefficient between the two sites potentially  
 635 confounds our interpretation of subsurface hydrologic controls on emergent hillslope length  
 636 and hydrological function, assuming the difference is due to a contrast in material prop-  
 637 erties rather than hydrology. Our estimated subsurface hydrological variables support  
 638 our perceptual model of how the sites should be different if they have coevolved with their  
 639 hydrology; lower transmissivity at Druids Run should lead to more surface runoff and  
 640 channel incision, and greater extent of variably saturated areas than the high transmis-  
 641 sivity conditions at Baisman Run. However, a higher streampower incision coefficient  
 642 may indicate that runoff is more effective at detaching and transporting sediment out  
 643 of the watershed at Druids Run, which could also lead to closer spacing of channels and  
 644 shorter hillslopes (Perron et al., 2008).

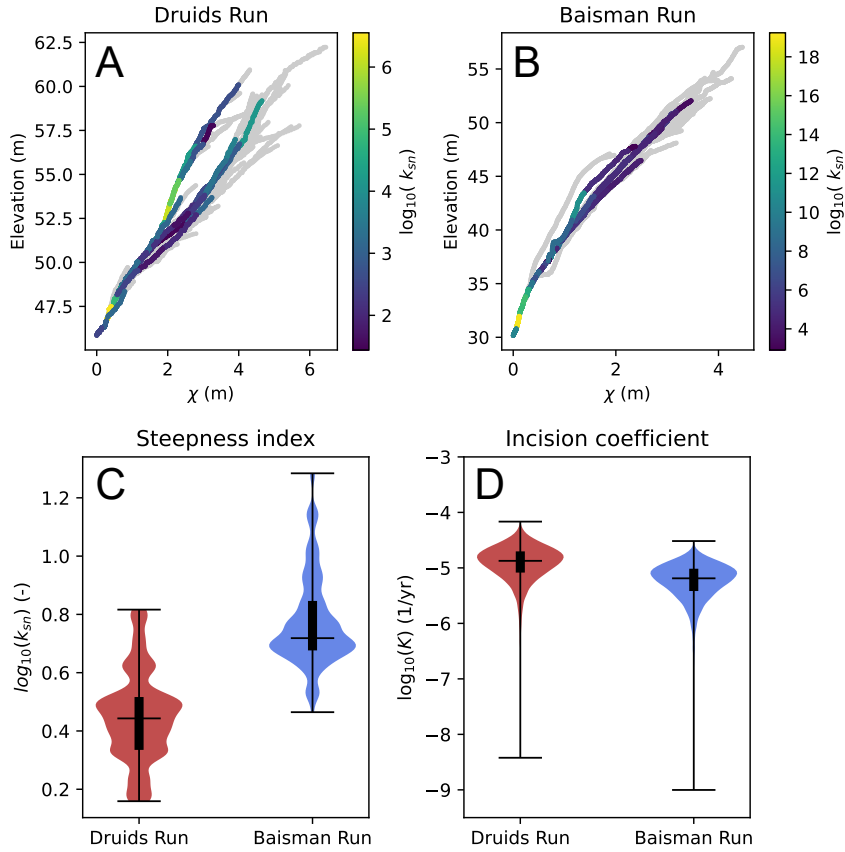


**Figure 11.**  $\chi$ -elevation plots for Druids Run (A) and Baisman Run (B) for a concavity index  $m/n = 0.5$ . Channel segments are colored by their steepness index  $k_{sn}$  where the upslope area is greater than the 40<sup>th</sup> watershed area percentile, and are otherwise gray. (C) the distributions of  $k_{sn}$  for the segments colored in (A) and (B), showing generally higher channel steepness at Baisman Run than Druids Run. (D) distributions of the streampower incision coefficient  $K$  from Monte Carlo simulations.  $k_{sn}$  scales inversely with the erodibility, such that the streampower incision coefficient is lower at Baisman Run than Druids Run.

645 To test whether subsurface hydrology is necessary and sufficient for explaining the  
 646 difference in variable source areas and hillslope length at the two sites, we ran four sim-  
 647 ulations, shown in Figure 12: two that represent our best estimates of hydrological and  
 648 geomorphic parameters as described above (DR-DR, BR-BR), and two where we swapped  
 649 the geomorphic parameters (DR-BR, BR-DR). Our best estimate cases helped discrim-  
 650 inate how well DupuitLEM can capture landscape geomorphic and hydrologic dynam-  
 651 ics at our sites. By comparing the best estimate simulations with simulations that have  
 652 the same hydrological parameters but swapped geomorphic parameters, we determined  
 653 whether geomorphic process rates alone explained the differences in morphology when  
 654 the landscape coevolves with hydrology. Due to uncertainties in initial conditions and  
 655 landscape history, we do not expect the simulation results to look exactly like Druids Run  
 656 or Baisman Run. Instead, we compared them on the basis of aggregate properties in-  
 657 cluding the hillslope length and relief, and saturation behavior. Beyond the direct site  
 658 comparison, this approach also allows for exploration of topographic sensitivity to sub-  
 659 surface properties in a realistic region of the DupuitLEM parameter space.

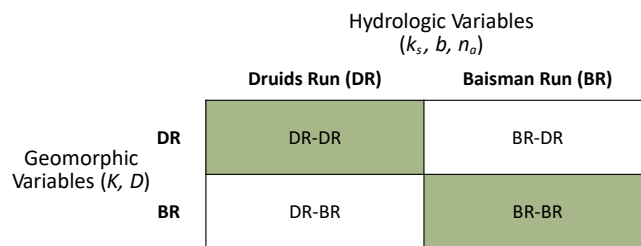


**Figure 12.** Four boxes indicating the four simulations we conducted. Colored boxes indicate the correctly matched hydrologic and geomorphic parameters, while white boxes indicate the ones in which the geomorphic variables are swapped. The listed hydrological and geomorphic variables are those that are varied, while all others are kept the same.

660 Lastly, we considered what happens when the differences in observed channel steep-  
 661 ness were due to differences in runoff ratio ( $Q_{max}^*$ ) rather than material properties ( $K$ ).  
 662 In our model formulation, determining the right value of  $Q_{max}^*$  should be an iterative  
 663 process, in which the value of  $Q_{max}^*$  is estimated in order to determine erodibility, the  
 664 model is run forward, the discharge and precipitation from the simulated landscape are  
 665 used to recalculate  $Q_{max}^*$ , and then the streampower incision coefficient is adjusted ac-  
 666 cordingly. This would be repeated until the estimated  $Q_{max}^*$  value matches the value pro-  
 667 duced by the simulation. If there is a mismatch, the channel steepness of the modeled  
 668 topography will be offset from that measured at the site. While we did not do a com-  
 669 plete iterative solution, we did adjust  $Q_{max}^*$  and  $K$  according to the results of our first  
 670 simulation.

### 671 3.3 Landscape evolution results

672 The landscape evolution model results showed subsurface hydrology has a signif-  
 673 icant effect on the morphology of emergent landscapes, and revealed the complexity of  
 674 interactions between hydrologic and geomorphic processes. However, the model was un-  
 675 able to faithfully reproduce the hillslope length, relief, and (for Druids run particularly)  
 676 important details of the hydrologic behavior.

677 We first simulated topography for the four cases presented in Figure 12, and an-  
 678 alyzed the hillslope properties and persistence of saturated areas using the same crite-

679 ria as we used for the field sites. The only necessary difference was that we identified chan-  
 680 nel heads using a threshold on topographic curvature ( $\nabla^2 z > 0.001$ ), because the DrE-  
 681 ICH algorithm performed poorly on our model simulations, which are much lower res-  
 682 olution than the lidar-derived DEMs. Because the transmissivity is the primary differ-  
 683 ence in hydrological variables, we call the cases with hydrology like Druids Run (DR-  
 684 DR and DR-BR) the low transmissivity cases, and cases with hydrology like Baisman  
 685 Run (BR-BR and BR-DR) the high transmissivity cases.

686 The most striking pattern in the hillshades shown in Figure 13A is that the low  
 687 transmissivity cases were substantially more dissected than the high transmissivity cases.  
 688 DR-DR and DR-BR, the two cases with hydrological parameters estimated for Druids  
 689 Run, have extensive fluvial dissection that extends onto hillslopes, which appears more  
 690 extensive than we observed at Druids Run. However, the broad undissected hillslopes  
 691 in BR-BR and BR-DR are similar to what we observed at Baisman Run. Despite some  
 692 visual similarities, Figure 13B–C shows that BR-BR and BR-DR cases tended to over-  
 693 predict hillslope length and relief. Also, contrary to our expectations, in the low trans-  
 694 missivity cases where the geomorphic properties have been swapped (DR-DR versus DR-  
 695 BR), the difference in hillslope length and relief appeared to be comparable to the dif-  
 696 ference between Baisman Run and Druids Run (for a better view of length and relief at  
 697 the field sites, see Figure 8). However, the presence of fluvial dissection broadly across  
 698 these modeled topographies makes direct comparison with our field sites more difficult.  
 699 In the high transmissivity cases, channels are clearly defined from hillslopes, but we have  
 700 a smaller sample from which to derive metrics. Hillslope length and relief appear to be  
 701 less sensitive to the difference in geomorphic variables than in the low transmissivity cases.

702 Swapping geomorphic parameters had a relatively minor effect on hydrological func-  
 703 tion. Figure 14A shows that simulations with swapped geomorphic parameters but the  
 704 same hydrologic parameters have very similar saturated area patterns, whereas there is  
 705 a substantial difference between simulations that have different hydrologic parameters.  
 706 The low transmissivity cases have large variably saturated areas that extend onto hill-  
 707 tops, as at Druids Run, though there are no hilltops that are classified as dry in the low  
 708 transmissivity cases. They also show more persistent saturation in valley bottoms and  
 709 zero-order basins than observed in Druids Run (Figure 14A–B). The saturated areas mod-  
 710 eled in the high transmissivity cases look very similar to those observed at Baisman Run,  
 711 where there is persistent saturation in valley bottoms and dry hilltops. Some channel  
 712 heads near the domain boundary of BR-BR even show wider seep-like channel heads, which  
 713 may be analogous to the saturated headwaters and springs seen at Baisman Run. The  
 714 fractional saturated areas are similar to those observed at the sites as well (Figure 14B).

715 Next we examined the emergent runoff ratio and adjusted the fluvial parameters  
 716 to account for the difference between the runoff ratio and the initial estimate of  $Q_{max}^*$ .  
 717 The emergent runoff ratio for the high transmissivity cases were 0.33 and 0.32 for BR-  
 718 BR and BR-DR respectively, which were very close to our initial estimate of 0.3, which  
 719 was the observed runoff ratio at Baisman Run. The difference in geomorphic paramet-  
 720 ers had little effect on emergent runoff ratio in these cases. In the low transmissivity  
 721 cases, the runoff ratio was significantly higher than our initial estimate of 0.3. We found  
 722 runoff ratios of 0.86 and 0.81 for DR-DR and DR-BR respectively. These values are again  
 723 not highly sensitive to the difference in geomorphic parameters, but both are substan-  
 724 tially higher than our initial estimate, and higher than our field estimate of 0.57 for Druid  
 725 Run. However, this is consistent with our observation that DR-DR and DR-BR have much  
 726 more extensive saturated areas than Druids Run. These higher runoff ratios suggest that  
 727 we should increase estimated  $Q_{max}^*$ , and therefore decrease the estimated  $K$  at Druids  
 728 Run. If we increase  $Q_{max}^*$  to 0.6, the corresponding  $K$  values is  $6.68e-6 \text{ yr}^{-1}$ , which is  
 729 within 3% of the  $K$  value we estimated for Baisman Run. The geomorphic results of this  
 730 increase are shown in Figure 15. The hydrologic effect of this increase is minimal, as shown  
 731 in Figure S2.

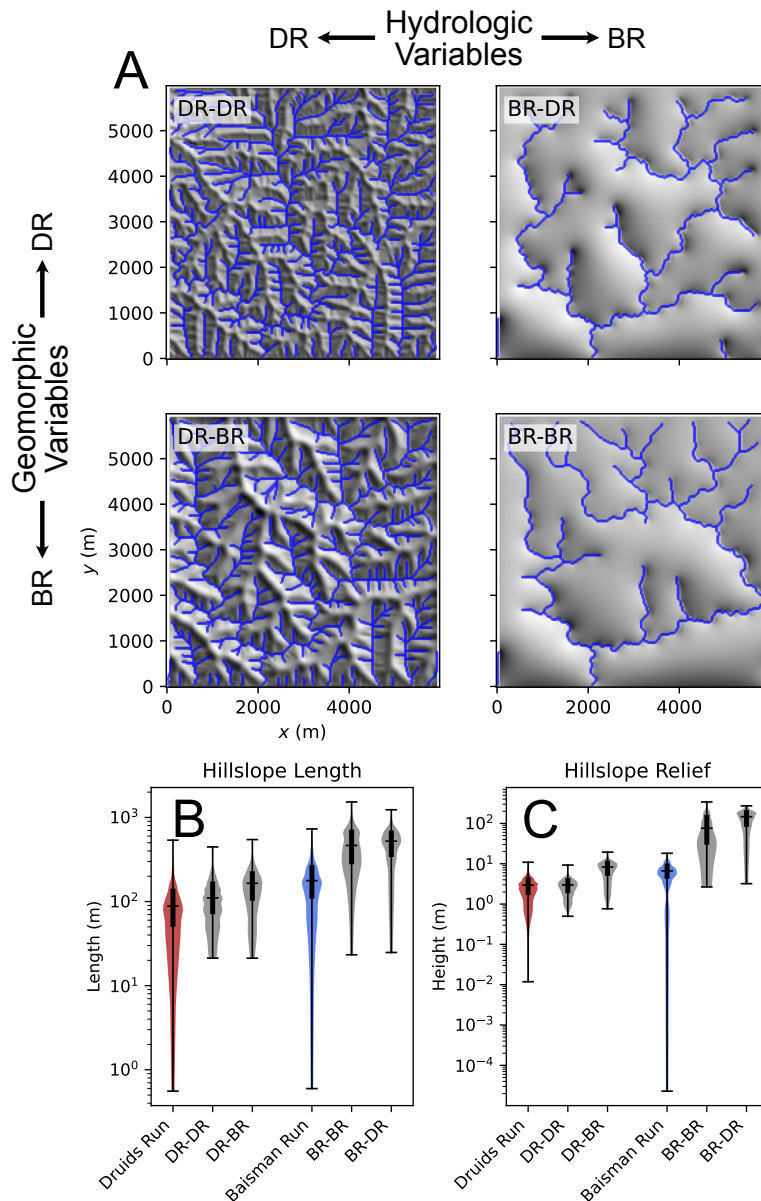


**Figure 13.** (A) Hillshades of model results in the same configuration as shown in Figure 12. Dissection is substantially higher in cases with Druids Run hydrological variables than Baisman Run hydrological variables. (B, C) Log-scaled violin plots of hillslope length and relief, comparing the field data (labelled “Druids Run” and “Baisman Run”) to the four modeled cases. Horizontal lines represent the maximum and minimum values, while the vertical bar represents the interquartile range.

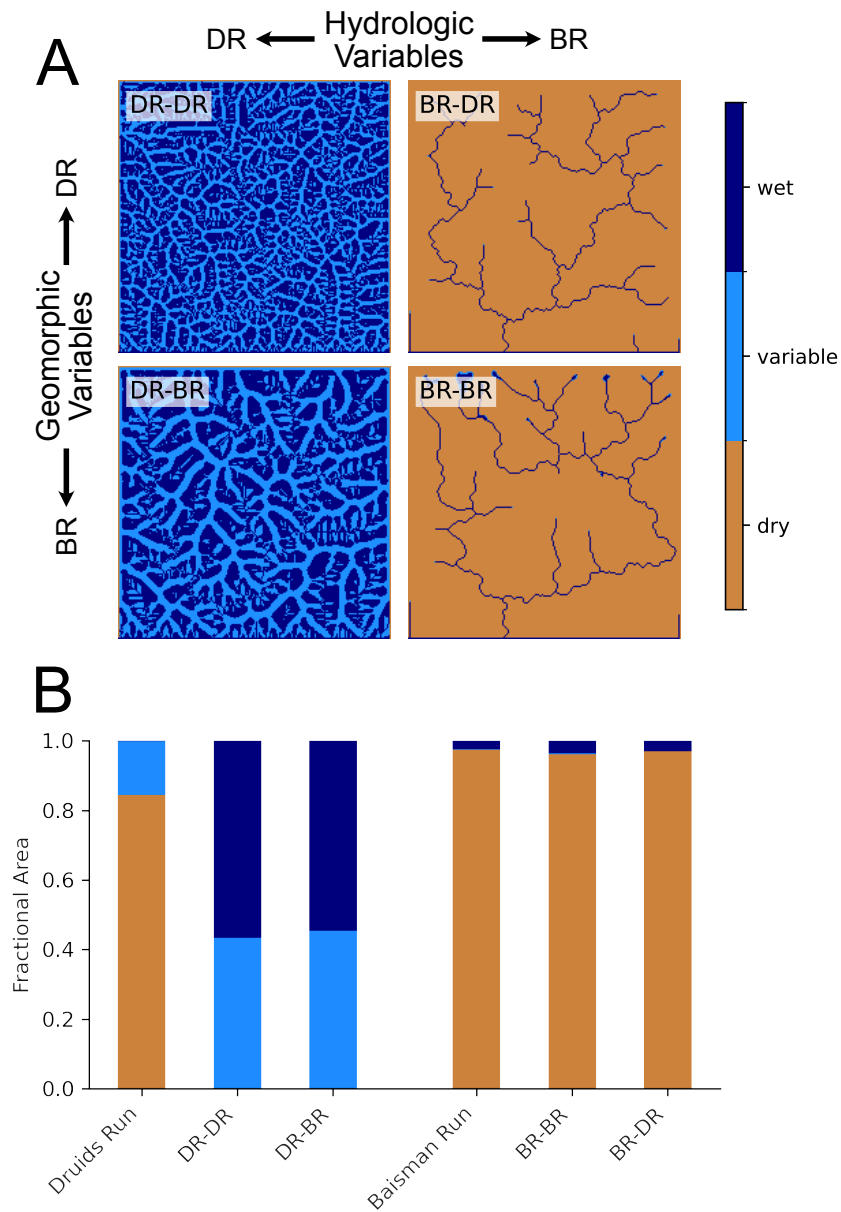


**Figure 14.** (A) Map view of saturated area classes for model results in the same configuration as shown in Figure 12 and Figure 13A. Saturated area behavior is not highly sensitive to swapping geomorphologic variables, while it is sensitive to swapping hydrological variables. (B) Fractional area that is classified as wet, variable, and saturated based on field data (labelled “Druids Run” and “Baisman Run”) and the four modeled cases. Cases that have the hydrological variables associated with Baisman Run appear similar to the field characteristics of Baisman Run. Cases that have the hydrological variables associated with Druids Run show more persistent saturation than the field characteristics of Druids Run.

Adjusting the streampower incision coefficient for differences in  $Q_{max}^*$  nearly eliminates the difference in emergent morphology and hydrology between cases with swapped geomorphic parameters. The hydrological function of the landscapes is very similar when geomorphic parameters are swapped, which is expected given that there was little difference in hydrological function between the original cases with swapped geomorphic parameters. The emergent runoff ratio for DR-DR is now 0.78, which is slightly lower than we calculated previously. The modeled topography looks very similar when geomorphic parameters are swapped, and distributions of hillslope length and relief are nearly identical (Figure 15). At least within the context of our model, this suggests that differences in geomorphic parameters are not sufficient to explain the differences between the sites. The results suggest that the difference in morphology between Druids Run and Baisman Run is strongly affected by the difference in their subsurface hydrology, as (1) the difference in transmissivity changes the extent of saturated areas and surface water on the landscape, which changes the proportion of the landscape that experiences fluvial erosion, and (2) higher runoff ratios increase the efficiency of water-driven sediment transport in areas where there is saturation, which further incises the landscape.

Our results also showed that there is more work to do to understand the controls on the geomorphic evolution of our sites. For instance, adjusting  $Q_{max}^*$  did not bring us closer to the true hillslope length and relief. Figure 16 shows how the true cases DR-DR and BR-BR compare to the hillslope length and relief of Druids Run and Baisman Run, respectively. The number in parentheses following the model label is the estimated value of  $Q_{max}^*$ . The values of hillslope length and relief from simulation DR-DR (0.6) were farther from the true values at Druids Run than those from simulation DR-DR (0.3). At the same time, we know that the channel steepness  $k_{sn}$  from the simulation DR-DR (0.3) will not match  $k_{sn}$  of Druids Run, because we overestimated the streampower incision coefficient  $K$  relative to the emergent value of  $Q_{max}^*$ . More work is needed to understand both the possible difference in other parameters (e.g., the denudation rate) and limitations of model structure for capturing our sites, but it is clear that the difference in the hydrology of the sites is an important component of their geomorphic evolution.

## 4 Discussion

### 4.1 The expression of subsurface hydrology in landscape evolution

Previous work on the role of transmissivity in topographic evolution (Luijendijk, 2022; Litwin et al., 2022, 2024) is a logical extension of the hydrological study of runoff generation, as sediment transport is an important consequence of runoff generation. It has only recently received attention, in part because considering the long-term effects of this coevolution is computationally intensive, and in part because it relies on subsurface properties that are hard to estimate. Available models also lack critical aspects of channel head formation, which would themselves require more thorough treatment of the conversion of rock to regolith (see Section 4.2.2). As a result, landscape evolution modelers typically select the minimally-complex model needed to explain their observations. As a result, they have often excluded subsurface hydrology, despite the widespread importance of subsurface flow for runoff generation (Wu et al., 2021). We have shown here that subsurface hydrology may be indispensable for understanding the evolution of some landscapes. The importance of subsurface runoff generation for a particular application of a landscape evolution model is dependent on the geologic and climatic setting, but also on the scale of interest. Studies focusing on watershed scales of 1-10s of kilometers may find that capturing subsurface flow is essential, while these details may be less important in the evolution of entire orogens, where the length of subsurface flow paths relevant to runoff generation is shorter than the scales of geomorphic interest.

We showed strong sensitivity of topography to subsurface hydrology for reasonable combinations of parameters, but also showed that there were limitations to how realis-

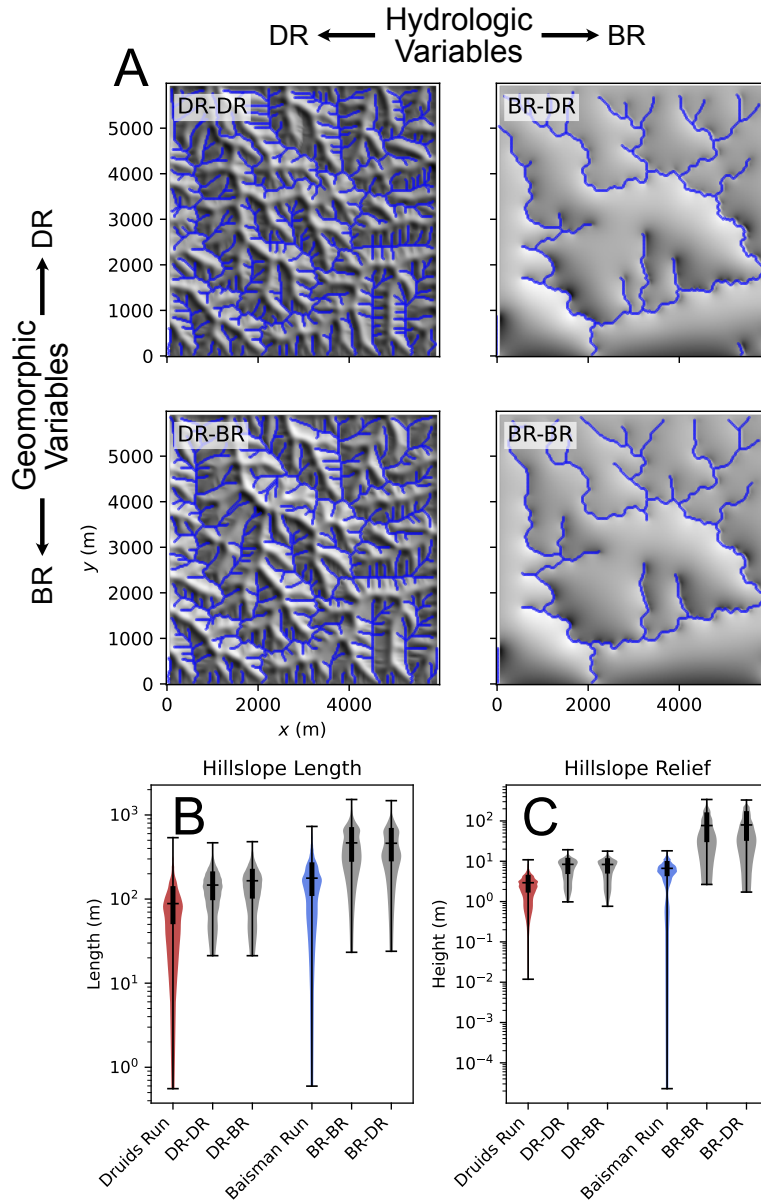


**Figure 15.** (A) Hillshades of model results in the same configuration as shown in Figure 12, only  $Q_{max}^* = 0.6$  was used to determine the streampower incision coefficient for cases with Druids Run geomorphic variables. Visual comparison of results suggests that the difference in hydrology between the two sites is the primary control on emergent morphology. (B, C) Violin plots of hillslope length and relief, comparing the field data (labelled “Druids Run” and “Baisman Run”) to the four modeled cases. There is little difference between simulations with swapped geomorphic variables (comparing down columns), while there is still substantial sensitivity to swapped hydrological variables (compare across rows). All four modeled cases still have length and relief greater than those observed in the field.



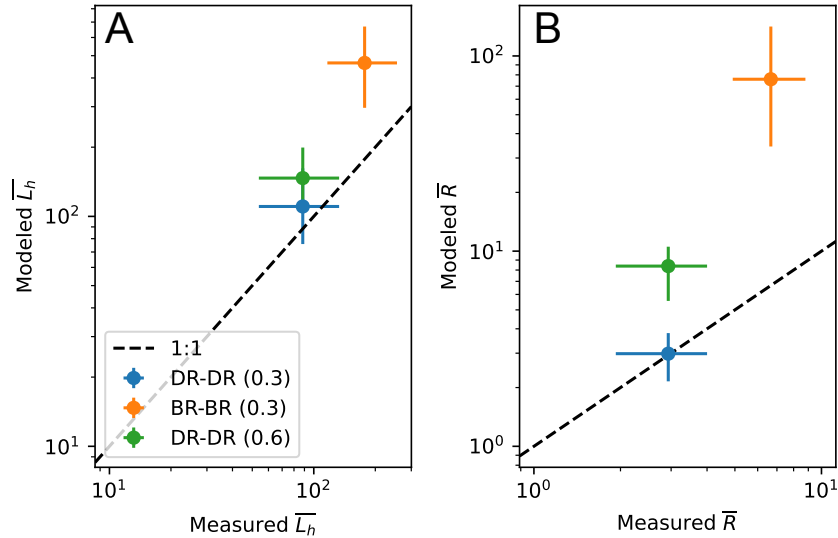


**Figure 16.** Modeled versus observed hillslope length (A) and hillslope relief (B). Results are only shown for the true cases (not the swapped parameter cases). The number following the simulation name is the value of  $Q_{max}^*$ . For Druids Run, simulations using both the original and updated estimates of  $Q_{max}^*$  are shown. The points are median values, and the error bars show the interquartile range.

783 tically DupuitLEM can capture our sites. We were able to make both of these assess-  
 784 ments in part because we had hydrologic as well as geomorphic observations. While many  
 785 studies have sought to test the sensitivity of landscape morphology to climate (e.g., Fer-  
 786 rier et al., 2013; Adams et al., 2020; Zavala et al., 2020), hydrological field data can re-  
 787 veal functional differences between sites due to subsurface properties that would be in-  
 788 distinguishable based on climate alone. Measurements of the location and magnitude of  
 789 runoff and erosion are likely the most relevant variables for such assessments. Discharge  
 790 records are widely available and can provide some indication on runoff generation mech-  
 791 anisms (McMillan, 2020). The addition of sediment concentration timeseries can enrich  
 792 discharge timeseries to provide a stronger link between runoff generation and erosion (Tolorza  
 793 et al., 2014). When possible, observations of runoff on foot, or remotely with cameras  
 794 or satellite platforms (Godsey & Kirchner, 2014; Antonelli et al., 2020; Dralle et al., 2023;  
 795 Harrison et al., 2020) can provide valuable comparisons to basin-integrated timeseries.  
 796 Geomorphic proxies may also be useful. Rossi et al. (2020) found that bedrock exposure,  
 797 as a proxy for low subsurface storage and infiltration capacity, explained variation in ex-  
 798 treme runoff events better than variation in precipitation across an elevation gradient  
 799 in the Colorado Front Range. Combinations of discharge, topographic analysis, and cos-  
 800 mogenic erosion rates have also allowed new examinations of channel head forming mech-  
 801 anisms that could be useful for informing future modelling (Harrison et al., 2020).

## 802 4.2 Parameter estimation and limits of DupuitLEM

803 While our results provide evidence for a critical link between subsurface hydrology  
 804 and landscape evolution, there are clear discrepancies between the characteristics  
 805 of Baisman Run and Druids Run that we observed and those we were able to model with  
 806 DupuitLEM. Some of these discrepancies could be due to our choice of model param-  
 807 eters, while others appear to be structural limitations of DupuitLEM.

#### 808 **4.2.1 Parameter uncertainty**

809 Our results here and in prior studies (Litwin et al., 2022, 2024) demonstrate that  
 810 emergent topography and hydrology are highly sensitive to transmissivity, so the accu-  
 811 racy of the transmissivity estimate is likely a factor in model-data discrepancies. Our  
 812 novel approach to estimate transmissivity relied on topographic index as a measure of  
 813 hydrological similarity (O’Loughlin, 1986; Beven & Kirkby, 1979). However, our results  
 814 showed that topographic index and discharge, when combined in Equation 7, were only  
 815 modestly good predictors of saturated area (Figure 9). Furthermore, topographic index  
 816 is a resolution-dependent quantity (Zhang & Montgomery, 1994), which means that the  
 817 resulting transmissivity that we calculate also depends on DEM resolution. While ac-  
 818 counting for this effect is unlikely to change the relative magnitudes of transmissivity be-  
 819 tween the sites, it may change the estimated values. This was a problem with calibrated  
 820 transmissivities in TOPMODEL as well (Beven, 1997), so some of the strategies that have  
 821 been devised to reduce the scale dependence in that context (e.g., Saulnier et al., 1997)  
 822 may be useful for improving our transmissivity estimates as well.

823 Our model results also showed that hillslope length and relief were too large in the  
 824 simulated landscapes regardless of transmissivity. This could suggest that the relative  
 825 magnitude of hillslope diffusivity to the fluvial erosion efficiency is too large (Perron et  
 826 al., 2008; Theodoratos et al., 2018). Our modelled cases are generally able to reproduce  
 827 observed hilltop curvature (Figure S3A), which suggests that the diffusivity is not the  
 828 primary issue. Modelled channel steepness, however, is systematically larger than the  
 829 channels from which the parameters were defined (Figure S3B). One likely issue that could  
 830 explain this discrepancy arises from using  $K$  estimates from 1D channel profiles in a 2D  
 831 model. Hillslopes in the 2D model contribute material to valleys that rivers must remove.  
 832 This decreases their erosional efficiency compared to what is expected when estimating  
 833  $K$  from a 1D profile in which the river only needs to erode at a rate  $U$  (Equation 16).  
 834 This topic requires further exploration than can be accommodated here, and will be cov-  
 835 ered in future work.

#### 836 **4.2.2 Process uncertainty**

837 While there are limitations to our ability to estimate transmissivity and other pro-  
 838 cess rates, we know that some key hydrological and geomorphic processes and features  
 839 are missing from our model. These may be the cause of the model’s inability to accu-  
 840 rately reproduce the length and relief at each site. DupuitLEM was designed to be a min-  
 841 imally complex representation of coupled hydrology and landscape evolution in humid  
 842 upland environments, and thus necessarily left many processes out that are relevant to  
 843 the particular sites we have discussed here.

844 A key hydrological limitation of our model is in the routing of surface water. It is  
 845 challenging to balance flow convergence and divergence in a single efficient algorithm (Pelletier,  
 846 2010). We use the D8 flow algorithm (O’Callaghan & Mark, 1984), which directs all flow  
 847 at a point to a single downslope node. This may be a key limitation for comparison with  
 848 Druids Run, where we observed saturation and runoff on divergent hillslopes. Our sim-  
 849 plifications in our vadose zone model also prevent evaporation or transpiration of wa-  
 850 ter from the saturated zone. Including it would decrease the proportion of the water-  
 851 shed that stays saturated during interstorm periods and decrease antecedent wetness when  
 852 storms arrive.

853 Our subsurface model was also limited to be spatially uniform and homogeneous.  
 854 We know this is not the case. In Baisman Run, deeply weathered zones under hillslopes  
 855 delay the arrival of hillslope water to streams and support baseflow, while a relatively  
 856 shallow subsurface in valley bottoms may increase the likelihood of overland flow in the  
 857 channels (Cosans, 2022; St. Clair et al., 2015). This pattern could increase flow persis-  
 858 tence and drainage dissection relative to a uniform subsurface. In contrast, very thin soils

859 on hillslopes at Druids Run allow saturation and overland flow to occur frequently, while  
 860 a more permeable valley bottom may increase the subsurface conveyance in valleys rel-  
 861 ative to the amount of water that remains after storms. Depending on how the ripar-  
 862 ian area is connected to the stream, it may also store more water that can be slowly re-  
 863 leased during interstorm periods. These patterns could increase or decrease saturated  
 864 areas and drainage dissection, depending on the extent of the riparian aquifer and its  
 865 stream connection.

866 In addition to shaping subsurface structure, weathering can also result in signif-  
 867 icant chemical denudation. DupuitLEM, like many geomorphic models, only treats phys-  
 868 ical erosion. Cleaves et al. (1974) studied the denudation of Pond Branch (a subwater-  
 869 shed of Baisman Run) and a small watershed on the on the Soldiers Delight Ultramafite  
 870 that is south of our site. On the basis of a geochemical mass balance, they estimated that  
 871 chemical weathering was responsible for approximately 90% of denudation in Soldiers  
 872 Delight at present, while it was responsible for approximately 50% of denudation at Pond  
 873 Branch. This could suggest a significant difference in interpretation of morphologic dif-  
 874 ferences. We discuss this further in A.

875 There are also limitations to the style of erosion considered by the model. In en-  
 876 vironments with humid climates and crystalline bedrock, seepage erosion at springs may  
 877 play an important role in channel network evolution, given that shear stress at channel  
 878 heads may not generally be high enough to incise bedrock alone (Dunne, 1990, 1980).  
 879 This could help explain why the drainage density in our model parameterized for Bais-  
 880 man Run is higher than that in the real watershed. A more thorough treatment of this  
 881 process would also require more consideration for weathering, which must ultimately sup-  
 882 ply material that can be transported at the low discharge rates found at channel heads.  
 883 Despite lacking this complexity, our model is still able to simulate some spring-like fea-  
 884 tures that are characteristic of Baisman Run. This suggests a degree of flexibility of the  
 885 streampower law, when coupled with the right discharge function.

## 886 5 Conclusions

887 The analysis of the two study sites and modeling with DupuitLEM presented here  
 888 support the idea that subsurface transmissivity is a major control on not only the hy-  
 889 drologic function of humid, soil-mantled landscapes, but also on their morphology. We  
 890 framed this paper with two hypotheses about how the morphology and hydrological func-  
 891 tion of two landscapes should be different, informed by understanding (gleaned from pre-  
 892 vious modeling studies) of how the subsurface could affect the coevolution of runoff and  
 893 topography. From field data, we found that both the hydrological function and morphol-  
 894 ogy aligned with our predictions; Druids Run, which has a thin permeable subsurface,  
 895 had more extensive variably saturated areas, more variable effective area contributing  
 896 runoff, and shorter hillslopes than Baisman Run, which has a deep permeable subsur-  
 897 face. A novel use of topography, saturation and discharge observations further showed  
 898 that the transmissivity was substantially higher at Baisman Run than Druids Run.

899 We parameterized a coupled groundwater landscape evolution model for each site  
 900 using field observations, topographic analysis, and literature values, and ran the model  
 901 to geomorphic steady state. We were able to simulate the broad dry hillslopes and per-  
 902 sistent saturated valley bottoms at Baisman Run, but substantially overpredicted sat-  
 903 uration at Druids Run. The model correctly predicted that hillslope length and relief  
 904 would be substantially larger in the high-transmissivity site (Baisman Run), but was un-  
 905 able to reproduce the actual hillslope length and relief: at both sites it predicted longer  
 906 and higher hillslopes. These differences may be due to issues related to uncertainty and  
 907 biases in parameter estimation, and to inadequate representation of the actual geomor-  
 908 phic processes operating at each site. However, the difference in geomorphic process rates  
 909 was not sufficient to explain the between-site difference in hillslope length or hydrolog-

ical function, suggesting that the morphologic differences between the sites could reasonably be attributed to subsurface transmissivity.

## Appendices

### A Geomorphic contrasts based on chemical denudation

Some recent work begins to provide a framework for understanding morphologic effects of chemical denudation. Ben-Asher et al. (2019) introduced a modification of the hillslope mass balance that includes chemical denudation in the form of a chemical depletion fraction (CDF). They showed that curvature should be reduced as the ratio of chemical to total denudation increases, assuming a constant hillslope diffusivity. Marcon (2019) applied this principle to several hillslopes on contrasting lithologies across the Piedmont, including sites on schist and serpentine bedrock. They found decreasing hilltop curvature with increasing CDF, where serpentine sites had the highest CDF and lowest hilltop curvatures. At our sites we found virtually no difference in hilltop curvature between lithologies. If the total denudation rate at both sites is indeed very similar, but chemical denudation is dramatically different, we are left with the conclusion that the identical curvature is a coincidence that arises from higher hillslope diffusivity  $D$  at Druids Run than Baisman Run. Further research, including updated denudation estimates specific to our sites, would be needed to draw further conclusions on chemical denudation rates and geomorphic consequences at our sites.

### 6 Open Research

All original data, model output, and scripts needed to process data and generate figures are archived on Zenodo (Litwin & Harman, 2024). The Python package DupuitLEM v1.1 (Litwin et al., 2023) contains the models and scripts used to generate and post-process the model output. Landlab v2.0 (Barnhart et al., 2020) is a core dependency of DupuitLEM.

### Acknowledgments

This work was supported by National Science Foundation grants EAR-2012264 and EAR-1654194. Model simulations were carried out at the Advanced Research Computing at Hopkins (ARCH) core facility (rockfish.jhu.edu), which is supported by the National Science Foundation (NSF) grant number OAC-1920103. We appreciate help in the field from Joseph Stanley. We thank Tom Dunne, Gordon Grant, and an anonymous reviewer for comments that led to significant improvements in this manuscript.

### References

- Adams, B. A., Whipple, K. X., Forte, A. M., Heimsath, A. M., & Hodges, K. V. (2020). Climate controls on erosion in tectonically active landscapes. *Science Advances*, *6*(42), eaaz3166. (Publisher: American Association for the Advancement of Science) doi: 10.1126/sciadv.aaz3166
- Antonelli, M., Glaser, B., Teuling, A. J., Klaus, J., & Pfister, L. (2020). Saturated areas through the lens: 1. Spatio-temporal variability of surface saturation documented through thermal infrared imagery. *Hydrological Processes*, *34*(6), 1310–1332. doi: 10.1002/hyp.13698
- Barnhart, K. R., Hutton, E. W. H., Tucker, G. E., Gasparini, N. M., Istanbuluoğlu, E., Hobbey, D. E. J., . . . Bandaragoda, C. (2020). Short communication: Landlab v2.0: A software package for Earth surface dynamics. *Earth Surface Dynamics*, *8*(2), 379–397. doi: 10.5194/esurf-8-379-2020

- 954 Bazilevskaya, E., Lebedeva, M., Pavich, M., Rother, G., Parkinson, D. Y., Cole, D.,  
 955 & Brantley, S. L. (2013). Where fast weathering creates thin regolith and slow  
 956 weathering creates thick regolith. *Earth Surface Processes and Landforms*,  
 957 *38*(8), 847–858. doi: 10.1002/esp.3369
- 958 Ben-Asher, M., Haviv, I., Roering, J. J., & Crouvi, O. (2019). The potential influ-  
 959 ence of dust flux and chemical weathering on hillslope morphology: Convex  
 960 soil-mantled carbonate hillslopes in the Eastern Mediterranean. *Geomorphol-  
 961 ogy*, *341*, 203–215. doi: 10.1016/j.geomorph.2019.05.021
- 962 Beven, K. (1997). TOPMODEL: A critique. *Hydrological Processes*, *11*(9), 1069–  
 963 1085. doi: 10.1002/(SICI)1099-1085(199707)11:9<1069::AID-HYP545>3.0.CO;  
 964 2-O
- 965 Beven, K., & Kirkby, M. (1979). A physically based, variable contributing area  
 966 model of basin hydrology. *Hydrological Sciences Bulletin*, *24*(1), 43–69. doi: 10  
 967 .1080/02626667909491834
- 968 Brantley, S. L., Eissenstat, D. M., Marshall, J. A., Godsey, S. E., Balogh-Brunstad,  
 969 Z., Karwan, D. L., . . . Weathers, K. C. (2017). Reviews and syntheses: On  
 970 the roles trees play in building and plumbing the critical zone. *Biogeosciences*,  
 971 *14*(22), 5115–5142. doi: 10.5194/bg-14-5115-2017
- 972 Cleaves, E. T. (1989). Appalachian Piedmont landscapes from the Permian to the  
 973 Holocene. *Geomorphology*, *2*(1), 159–179. doi: 10.1016/0169-555X(89)90010  
 974 -X
- 975 Cleaves, E. T., Fisher, D. W., & Bricker, O. P. (1974). Chemical Weathering of Ser-  
 976 pentinite in the Eastern Piedmont of Maryland. *GSA Bulletin*, *85*(3), 437–444.  
 977 doi: 10.1130/0016-7606(1974)85<437:CWOSIT>2.0.CO;2
- 978 Cleaves, E. T., Godfrey, A. E., & Bricker, O. P. (1970). Geochemical Balance of  
 979 a Small Watershed and Its Geomorphic Implications. *GSA Bulletin*, *81*(10),  
 980 3015–3032. doi: 10.1130/0016-7606(1970)81[3015:GBOASW]2.0.CO;2
- 981 Clubb, F. J., Mudd, S. M., Milodowski, D. T., Hurst, M. D., & Slater, L. J. (2014).  
 982 Objective extraction of channel heads from high-resolution topographic data.  
 983 *Water Resources Research*, *50*(5), 4283–4304. doi: 10.1002/2013WR015167
- 984 Collins, D. B. G., & Bras, R. L. (2010). Climatic and ecological controls of equi-  
 985 librium drainage density, relief, and channel concavity in dry lands. *Water Re-  
 986 sources Research*, *46*(4). doi: 10.1029/2009WR008615
- 987 Cosans, C. L. (2022). *Landscape Structure, Flow Path, and Transport Co-Evolution  
 988 in the Deeply Weathered Piedmont* (Thesis). Johns Hopkins University.
- 989 Crowley, W. P., Reinhardt, J., & Cleaves, E. T. (1975). *Geologic map of the Cock-  
 990 eysville quadrangle* (QA-3 ed.). Baltimore, Maryland: Maryland Geological  
 991 Survey.
- 992 Dralle, D. N., Lapedes, D. A., Rempe, D. M., & Hahm, W. J. (2023). Mapping  
 993 Surface Water Presence and Hyporheic Flow Properties of Headwater Stream  
 994 Networks With Multispectral Satellite Imagery. *Water Resources Research*,  
 995 *59*(9), e2022WR034169. doi: 10.1029/2022WR034169
- 996 Dunne, T. (1980). Formation and controls of channel networks. *Progress in Physical  
 997 Geography: Earth and Environment*, *4*(2), 211–239. (Publisher: SAGE Publi-  
 998 cations Ltd) doi: 10.1177/030913338000400204
- 999 Dunne, T. (1990). Chapter 1. Hydrology mechanics, and geomorphic implications  
 1000 of erosion by subsurface flow. In *Geological Society of America Special Papers*  
 1001 (Vol. 252, pp. 1–28). Geological Society of America. doi: 10.1130/SPE252-p1
- 1002 Eagleson, P. (1978). Introduction to Water Balance Dynamics. *Water Resources Re-  
 1003 search*, *14*(5), 705–712. doi: 10.1016/j.compchemeng.2012.11.011
- 1004 Ferrier, K. L., Huppert, K. L., & Perron, J. T. (2013). Climatic control of bedrock  
 1005 river incision. *Nature*, *496*(7444), 206–209. (Publisher: Nature Publishing  
 1006 Group) doi: 10.1038/nature11982
- 1007 Godsey, S. E., & Kirchner, J. W. (2014). Dynamic, discontinuous stream net-  
 1008 works: Hydrologically driven variations in active drainage density, flowing

- 1009 channels and stream order. *Hydrological Processes*, 28(23), 5791–5803. doi:  
1010 10.1002/hyp.10310
- 1011 Grieve, S. W., Mudd, S. M., & Hurst, M. D. (2016). How long is a hillslope? *Earth*  
1012 *Surface Processes and Landforms*, 41(8), 1039–1054. doi: 10.1002/esp.3884
- 1013 Guice, G. L., Ackerson, M. R., Holder, R. M., George, F. R., Browning-Hanson,  
1014 J. F., Burgess, J. L., . . . Viete, D. R. (2021). Suprasubduction zone ophiolite  
1015 fragments in the central Appalachian orogen: Evidence for mantle and Moho  
1016 in the Baltimore Mafic Complex (Maryland, USA). *Geosphere*, 17(2), 561–581.  
1017 doi: 10.1130/GES02289.1
- 1018 Harel, M. A., Mudd, S. M., & Attal, M. (2016). Global analysis of the stream power  
1019 law parameters based on worldwide 10Be denudation rates. *Geomorphology*,  
1020 268, 184–196. doi: 10.1016/j.geomorph.2016.05.035
- 1021 Harrison, E. J., Brocard, G. Y., Gasparini, N. M., Lyons, N. J., & Willenbring,  
1022 J. K. (2020). Seepage erosion in the Luquillo Mountains, Puerto Rico,  
1023 relict landscapes. *Journal of Geophysical Research: Earth Surface*, 125(6),  
1024 e2019JF005341. doi: 10.1029/2019JF005341
- 1025 Hewlett, J. D., & Hibbert, A. R. (1967). Factors affecting the response of small wa-  
1026 tersheds to precipitation in humid areas. In *Int. Symp. Forest Hydrology*. doi:  
1027 10.1177/0309133309338118
- 1028 Horton, R. E. (1945). Erosional development of streams and their drainage basins;  
1029 hydrophysical approach to quantitative morphology. *GSA Bulletin*, 56(3), 275–  
1030 370. doi: 10.1130/0016-7606(1945)56[275:EDOSAT]2.0.CO;2
- 1031 Hurst, M. D., Mudd, S. M., Walcott, R., Attal, M., & Yoo, K. (2012). Us-  
1032 ing hilltop curvature to derive the spatial distribution of erosion rates.  
1033 *Journal of Geophysical Research: Earth Surface*, 117(F2), n/a-n/a. doi:  
1034 10.1029/2011jf002057
- 1035 Jencso, K. G., & McGlynn, B. L. (2011). Hierarchical controls on runoff generation:  
1036 Topographically driven hydrologic connectivity, geology, and vegetation. *Water*  
1037 *Resources Research*, 47(11). doi: 10.1029/2011WR010666
- 1038 Johnson, A. (1967). *Specific yield: Compilation of specific yields for various materi-*  
1039 *als* (USGS Numbered Series No. 1662-D). Washington, D.C.: U.S. Government  
1040 Printing Office. doi: 10.3133/wsp1662D
- 1041 Litwin, D. G., Barnhart, K. R., Tucker, G. E., & Harman, C. J. (2023). *DupuitLEM:*  
1042 *groundwater landscape evolution with landlab [software]*. Zenodo. doi: 10.5281/  
1043 zenodo.7620978
- 1044 Litwin, D. G., & Harman, C. J. (2024). *Data and model output for "Evidence of*  
1045 *subsurface control on the coevolution of hillslope morphology and runoff genera-*  
1046 *tion" [Dataset]*. Zenodo. doi: 10.5281/zenodo.10624746
- 1047 Litwin, D. G., Tucker, G. E., Barnhart, K. R., & Harman, C. J. (2022). Groundwa-  
1048 ter affects the geomorphic and hydrologic properties of coevolved landscapes.  
1049 *Journal of Geophysical Research: Earth Surface*, 127(1), e2021JF006239. doi:  
1050 10.1029/2021JF006239
- 1051 Litwin, D. G., Tucker, G. E., Barnhart, K. R., & Harman, C. J. (2024). Catchment  
1052 coevolution and the geomorphic origins of variable source area hydrology. *Wa-*  
1053 *ter Resources Research*, 60(6), e2023WR034647. doi: 10.1029/2023WR034647
- 1054 Luijendijk, E. (2022). Transmissivity and groundwater flow exert a strong influence  
1055 on drainage density. *Earth Surface Dynamics*, 10(1), 1–22. doi: 10.5194/esurf  
1056 -10-1-2022
- 1057 Luo, W., Jasiewicz, J., Stepinski, T., Wang, J., Xu, C., & Cang, X. (2016). Spatial  
1058 association between dissection density and environmental factors over the en-  
1059 tire conterminous United States. *Geophysical Research Letters*, 43(2), 692–700.  
1060 doi: 10.1002/2015GL066941
- 1061 Marcon, V. (2019). *The effect of lithology on (bio) geochemical weathering: sand-*  
1062 *stone to serpentinite}* (Unpublished doctoral dissertation). The Pennsylvania  
1063 State University, State College, PA.

- 1064 McMillan, H. (2020). Linking hydrologic signatures to hydrologic processes: A re-  
 1065 view. *Hydrological Processes*, *34*(6), 1393–1409. doi: 10.1002/hyp.13632
- 1066 Mudd, S., Clubb, F., Grieve, S., Milodowski, D., Gailleton, B., Hurst, M., . . . Hut-  
 1067 ton, E. (2022). *LSDtopotools/LSDTopoTools2: LSDTopoTools2 v0.7*. Zenodo.  
 1068 doi: 10.5281/ZENODO.3245040
- 1069 Mudd, S. M., Attal, M., Milodowski, D. T., Grieve, S. W. D., & Valters, D. A.  
 1070 (2014). A statistical framework to quantify spatial variation in channel gradi-  
 1071 ents using the integral method of channel profile analysis. *Journal of Geophysi-  
 1072 cal Research: Earth Surface*, *119*(2), 138–152. doi: 10.1002/2013JF002981
- 1073 NOAA. (2024). *NOAA atlas 14 point precipitation frequency estimates: MD*. Re-  
 1074 trieved 2024-01-11, from [https://hdsc.nws.noaa.gov/pfds/pfds\\_map\\_cont](https://hdsc.nws.noaa.gov/pfds/pfds_map_cont.html?bkmrk=md)  
 1075 [.html?bkmrk=md](https://hdsc.nws.noaa.gov/pfds/pfds_map_cont.html?bkmrk=md)
- 1076 O’Callaghan, J. F., & Mark, D. M. (1984). The extraction of drainage networks  
 1077 from digital elevation data. *Computer Vision, Graphics, & Image Processing*.  
 1078 doi: 10.1016/S0734-189X(84)80011-0
- 1079 O’Loughlin, E. M. (1986). Prediction of Surface Saturation Zones in Natural Catch-  
 1080 ments by Topographic Analysis. *Water Resources Research*, *22*(5), 794–804.
- 1081 Pavich, M. J. (1989). Regolith residence time and the concept of surface age of  
 1082 the Piedmont “Peneplain”. *Geomorphology*, *2*(1), 181–196. doi: 10.1016/0169-  
 1083 -555X(89)90011-1
- 1084 Pelletier, J. D. (2010). Minimizing the grid-resolution dependence of flow-routing al-  
 1085 gorithms for geomorphic applications. *Geomorphology*, *122*(1), 91–98. doi: 10-  
 1086 .1016/j.geomorph.2010.06.001
- 1087 Perron, J. T., Dietrich, W. E., & Kirchner, J. W. (2008). Controls on the spacing of  
 1088 first-order valleys. *Journal of Geophysical Research: Earth Surface*, *113*(4), 1–  
 1089 21. doi: 10.1029/2007JF000977
- 1090 Perron, J. T., & Royden, L. (2013). An integral approach to bedrock river profile  
 1091 analysis. *Earth Surface Processes and Landforms*, *38*(6), 570–576. doi: 10  
 1092 .1002/esp.3302
- 1093 Portenga, E. W., Bierman, P. R., Trodick, C. D., Jr., Greene, S. E., DeJong, B. D.,  
 1094 Rood, D. H., & Pavich, M. J. (2019). Erosion rates and sediment flux within  
 1095 the Potomac River basin quantified over millennial timescales using beryllium  
 1096 isotopes. *GSA Bulletin*, *131*(7-8), 1295–1311. doi: 10.1130/B31840.1
- 1097 Prancevic, J. P., & Kirchner, J. W. (2019). Topographic controls on the extension  
 1098 and retraction of flowing streams. *Geophysical Research Letters*, *0*(0). doi: 10  
 1099 .1029/2018GL081799
- 1100 Putnam, S. M. (2018). *The influence of landscape structure on storage and stream-  
 1101 flow generation in a Piedmont catchment* (Thesis). Johns Hopkins University.
- 1102 Roering, J. J., Perron, J. T., & Kirchner, J. W. (2007). Functional relationships  
 1103 between denudation and hillslope form and relief. *Earth and Planetary Science  
 1104 Letters*, *264*(1), 245–258. doi: 10.1016/j.epsl.2007.09.035
- 1105 Rossi, M. W., Anderson, R. S., Anderson, S. P., & Tucker, G. E. (2020). Orographic  
 1106 Controls on Subdaily Rainfall Statistics and Flood Frequency in the Colorado  
 1107 Front Range, USA. *Geophysical Research Letters*, *47*(4), e2019GL085086. doi:  
 1108 10.1029/2019GL085086
- 1109 Sangireddy, H., Carothers, R. A., Stark, C. P., & Passalacqua, P. (2016). Controls  
 1110 of climate, topography, vegetation, and lithology on drainage density extracted  
 1111 from high resolution topography data. *Journal of Hydrology*, *537*, 271–282.  
 1112 doi: 10.1016/j.jhydrol.2016.02.051
- 1113 Sauer, V. B., & Meyer, R. W. (1992). *Determination of error in individual discharge  
 1114 measurements* (Tech. Rep. No. 92–144). U.S. Geological Survey.
- 1115 Saulnier, G.-M., Obled, C., & Beven, K. (1997). Analytical compensation between  
 1116 DTM grid resolution and effective values of saturated hydraulic conductivity  
 1117 within the TOPMODEL framework. *Hydrological Processes*, *11*(9), 1331–1346.  
 1118 doi: 10.1002/(SICI)1099-1085(199707)11:9<1331::AID-HYP563>3.0.CO;2-9

- 1119 Schenk, H. J. (2008). The Shallowest Possible Water Extraction Profile: A Null  
 1120 Model for Global Root Distributions. *Vadose Zone Journal*, 7(3), 1119–1124.  
 1121 doi: 10.2136/vzj2007.0119
- 1122 Schmadel, N. M., Neilson, B. T., & Stevens, D. K. (2010, November). Approaches to  
 1123 estimate uncertainty in longitudinal channel water balances. *Journal of Hydrol-*  
 1124 *ogy*, 394(3), 357–369. doi: 10.1016/j.jhydrol.2010.09.011
- 1125 Staff, S. S., & Natural Resources Conservation Service, United States  
 1126 Department of Agriculture. (2023). *Web Soil Survey*.  
 1127 <https://websoilsurvey.sc.egov.usda.gov/App/WebSoilSurvey.aspx>.
- 1128 St. Clair, J., Moon, S., Holbrook, W. S., Perron, J. T., Riebe, C. S., Martel, S. J.,  
 1129 ... De Richter, D. B. (2015). Geophysical imaging reveals topographic  
 1130 stress control of bedrock weathering. *Science*, 350(6260), 534–538. doi:  
 1131 10.1126/science.aab2210
- 1132 Theodoratos, N., Seybold, H., & Kirchner, J. W. (2018). Scaling and similarity of  
 1133 a stream-power incision and linear diffusion landscape evolution model. *Earth*  
 1134 *Surface Dynamics*, 6(3), 779–808. doi: 10.5194/esurf-6-779-2018
- 1135 Tolorza, V., Carretier, S., Andermann, C., Ortega-Culaciati, F., Pinto, L., & Mar-  
 1136 dones, M. (2014). Contrasting mountain and piedmont dynamics of sediment  
 1137 discharge associated with groundwater storage variation in the Biobío River.  
 1138 *Journal of Geophysical Research: Earth Surface*, 119(12), 2730–2753. doi:  
 1139 10.1002/2014JF003105
- 1140 Troch, P. A., Lahmers, T., Meira, A., Mukherjee, R., Pedersen, J. W., Roy, T., &  
 1141 Valdes-Pineda, R. (2015). Catchment coevolution: A useful framework for im-  
 1142 proving predictions of hydrological change? *Water Resources Research*, 51(7),  
 1143 4903–4922. doi: 10.1002/2015WR017032
- 1144 Wu, S., Zhao, J., Wang, H., & Sivapalan, M. (2021). Regional Patterns and  
 1145 Physical Controls of Streamflow Generation Across the Conterminous  
 1146 United States. *Water Resources Research*, 57(6), e2020WR028086. doi:  
 1147 10.1029/2020WR028086
- 1148 Yoshida, T., & Troch, P. A. (2016). Coevolution of volcanic catchments in Japan.  
 1149 *Hydrology and Earth System Sciences*, 20(3), 1133–1150. doi: 10.5194/hess-20-  
 1150 -1133-2016
- 1151 Zavala, V., Carretier, S., & Bonnet, S. (2020). Influence of orographic precipita-  
 1152 tion on the topographic and erosional evolution of mountain ranges. *Basin Re-*  
 1153 *search*, 32(6), 1574–1599. (Publisher: European Association of Geoscientists &  
 1154 Engineers) doi: 10.1111/bre.12443
- 1155 Zhang, W., & Montgomery, D. R. (1994). Digital elevation model grid size, land-  
 1156 scape representation, and hydrologic simulations. *Water Resources Research*,  
 1157 30(4), 1019–1028. doi: 10.1029/93WR03553